Behavioral/Cognitive

Neuroticism/Negative Emotionality Is Associated with Increased Reactivity to Uncertain Threat in the Bed Nucleus of the Stria Terminalis, Not the Amygdala

Shannon E. Grogans,[1] Juyoen Hur,[2] Matthew G. Barstead,[3] Allegra S. Anderson,[4] Samiha Islam,[5] Hyung Cho Kim,[1,6] Manuel Kuhn,[7] Rachael M. Tillman,[8] Andrew S. Fox,[9,10] Jason F. Smith,[1]* Kathryn A. DeYoung,[1]* and Alexander J. Shackman[1,6,11]*

[1]Department of Psychology, University of Maryland, College Park, Maryland 20742, [2]Department of Psychology, Yonsei University, Seoul 03722, Republic of Korea, [3]Dead Reckoning Analytics & Consulting, College Park, Maryland 20740, [4]Department of Psychological Sciences, Vanderbilt University, Nashville, Tennessee 37240, [5]Department of Psychology, University of Pennsylvania, Philadelphia, Pennsylvania 19104, [6]Neuroscience and Cognitive Science Program, University of Maryland, College Park, Maryland 20742, [7]Center for Depression, Anxiety and Stress Research, McLean Hospital, Harvard Medical School, Belmont, Massachusetts 02478, [8]Children's National Hospital, Washington, DC 20010, [9]Department of Psychology, University of California, Davis, California 95616, [10]California National Primate Research Center, University of California, Davis, California 95616, and [11]Maryland Neuroimaging Center, University of Maryland, College Park, Maryland 20742

Neuroticism/negative emotionality (N/NE)—the tendency to experience anxiety, fear, and other negative emotions—is a fundamental dimension of temperament with profound consequences for health, wealth, and well-being. Elevated N/NE is associated with a panoply of adverse outcomes, from reduced socioeconomic attainment to psychiatric illness. Animal research suggests that N/NE reflects heightened reactivity to uncertain threat in the bed nucleus of the stria terminalis (BST) and central nucleus of the amygdala (Ce), but the relevance of these discoveries to humans has remained unclear. Here we used a novel combination of psychometric, psychophysiological, and neuroimaging approaches to test this hypothesis in an ethnoracially diverse, sex-balanced sample of 220 emerging adults selectively recruited to encompass a broad spectrum of N/NE. Cross-validated robust-regression analyses demonstrated that N/NE is preferentially associated with heightened BST activation during the uncertain anticipation of a genuinely distressing threat (aversive multimodal stimulation), whereas N/NE was unrelated to BST activation during certain-threat anticipation, Ce activation during either type of threat anticipation, or BST/Ce reactivity to threat-related faces. It is often assumed that different threat paradigms are interchangeable assays of individual differences in brain function, yet this has rarely been tested. Our results revealed negligible associations between BST/Ce reactivity to the anticipation of threat and the presentation of threat-related faces, indicating that the two tasks are nonfungible. These observations provide a framework for conceptualizing emotional traits and disorders; for guiding the design and interpretation of biobank and other neuroimaging studies of psychiatric risk, disease, and treatment; and for refining mechanistic research.

Key words: bed nucleus of the stria terminalis (BST/BNST); extended amygdala; fear and anxiety; neuroticism; temperament and personality

Significance Statement

Neuroticism/negative emotionality (N/NE) is a core dimension of mammalian temperament. Elevated levels of N/NE confer risk for a panoply of adversities—from reduced wealth and divorce to depression and death—yet the underlying neurobiology remains unclear. Here we show that N/NE is associated with heightened activation in the bed nucleus of the stria terminalis (BST) during the uncertain anticipation of a genuinely distressing threat. In contrast, N/NE was unrelated to BST reactivity during the certain anticipation of threat or the acute presentation of "threat-related" faces, two popular probes of the emotional brain. These findings refine our understanding of what has been termed the single-most important psychological risk factor in public health, with implications for ongoing biobank and therapeutics research.

Introduction

Individual differences in neuroticism/negative emotionality (N/NE)—the tendency to experience anxiety and other negative emotions—have profound consequences for health, wealth, and well-being (Shackman et al., 2016). Individuals with a more negative disposition show reduced socioeconomic attainment and are more likely to experience interpersonal conflict, loneliness, unemployment, and divorce; to engage in unhealthy behaviors; to develop pathological anxiety and depression; to become physically sick; and to die prematurely (Hur et al., 2019; Conway et al., in press). N/NE has been conceptualized as the single-most important psychological risk factor in public health, yet the underlying neurobiology remains surprisingly speculative (Lahey, 2009).

N/NE is thought to reflect a neurobiological tendency to overreact to threat, stressors, and other "trait-relevant" challenges (Shackman et al., 2016; Wrzus et al., 2021). Although a number of circuits have been implicated, the central extended amygdala (EAc)—including the central nucleus of the amygdala (Ce) and bed nucleus of the stria terminalis (BST)—has received the most empirical scrutiny and occupies a privileged position in most theoretical models (Fox et al., 2015b; DeYoung et al., 2022; Kagan, 2022). Mechanistic work demonstrates that the EAc is critical for orchestrating defensive responses to a variety of threats in humans and other animals (Fox and Shackman, 2019; Zhu et al., 2024). Neuroimaging studies in monkeys show that Ce and BST reactivity to uncertain threat covaries with trait-like variation in anxious temperament and behavioral inhibition, core facets of N/NE (Fox et al., 2015a; Shackman et al., 2017). But the relevance of these discoveries to humans remains unclear. Only a handful of human studies have used genuinely distressing threats to assess relations between N/NE and EAc function, and most have focused exclusively on the amygdala proper (Table 1). Even less is known about the BST. Only one small-scale study has directly addressed this question, providing preliminary evidence that individuals with a more negative disposition show heightened BST activation during the uncertain anticipation of aversive stimulation (Somerville et al., 2010). Although modest samples and a lack of attention to the BST preclude decisive inferences, these observations motivate the hypothesis that N/NE reflects heightened recruitment of the BST, and possibly the Ce, during the anticipation of aversive stimulation and suggest that these associations may be more pronounced when threat is uncertain.

Here we used fMRI to quantify EAc reactivity to a genuinely distressing threat-anticipation paradigm and test its relevance to N/NE in an ethnoracially diverse sample of 220 emerging adults (Figs. 1, 2). Participants were selectively recruited from a pool of 6,594 prescreened individuals, ensuring a broad spectrum of N/NE. Prior neuroimaging studies of N/NE have relied on overly optimistic analytic approaches (Marek et al., 2022). Here we used anatomically defined Ce and BST regions of interest (ROIs) and cross-validated robust estimates of brain–temperament associations (Fig. 1). To enhance power, we leveraged a composite measure of N/NE—aggregated across two scales and three measurement occasions—to minimize fluctuations in responding (Nikolaidis et al., 2022; Roemer et al., in press; Fig. 3). Hypotheses and approach were preregistered.

To provide a more direct link with ongoing research, we performed parallel analyses using data from an overlapping sample that completed an emotional-faces paradigm (Fig. 4). Variants of this paradigm are widely used in biobank research, often in the guise of assessing Research Domain Criteria "Negative Valence Systems" (Tozzi et al., 2020; Grogans et al., 2022). Although photographs of "threat-related" facial expressions robustly activate the EAc, they do not elicit substantial distress and are better conceptualized as an index of threat perception (Hur et al., 2019). The inclusion of the two threat paradigms also allowed us to test whether they are statistically interchangeable. It is often tacitly assumed that different tasks targeting a common function (e.g., "threat") are more or less equivalent probes of individual differences in brain function. Yet this assumption of convergent validity has rarely been examined empirically, never in a large sample, and never in the BST (Villalta-Gil et al., 2017).

Materials and Methods

Overview

As part of a recently completed prospective-longitudinal study focused on individuals at risk for the development of internalizing disorders (R01-MH107444), we used well-established psychometric measures of N/NE to screen 6,594 first-year university students (57.1% female; 59.0% White, 19.0% Asian, 9.9% African American, 6.3% Hispanic, 5.8% Multiracial/Other; $M = 19.2$ years; SD = 1.1 years; Shackman et al., 2018). Screening data were stratified into quartiles (top quartile, middle quartiles, bottom quartile), separately for males and females. Individuals who met preliminary inclusion criteria were independently and randomly recruited via email from each of the resulting six strata. Given our focus on psychiatric risk, approximately half the participants were recruited from the top quartile, with the remainder split between the middle and bottom quartiles (i.e., 50% high, 25% medium, and 25% low). This enabled us to sample a broad spectrum of N/NE without gaps or discontinuities—in contrast to prior work focused on convenience samples (Charpentier et al., 2021)—while balancing the inclusion of men and women (compare Fig. 1). Simulation work suggests that this oversampling ("enrichment") approach does not bias statistical tests to a degree that would compromise their validity (Hauner et al., 2014). All participants had normal or corrected-to-normal color vision and reported the absence of lifetime neurological symptoms, pervasive developmental disorder, very premature birth, medical conditions that would contraindicate MRI, and prior experience with noxious electrical stimulation. All participants were free from a lifetime history of psychotic and bipolar disorders; a current diagnosis of a mood, anxiety, or trauma disorder (past 2 months); severe substance abuse; active suicidality; and ongoing psychiatric treatment as determined by an experienced, master's-level diagnostician using the Structured Clinical Interview for DSM-5 (First et al., 2015). Other-specified internalizing diagnoses were not excluded. Participants provided informed written consent, and all procedures were approved by the Institutional Review Board at the University of Maryland, College Park (Protocol Number 659385). Data from this study were featured in prior work focused on relations between personality and the longitudinal course of internalizing symptoms (Conway et al., in press), validation of the threat-anticipation paradigm (Hur et al., 2020b; Shackman et al., in press), relations between social anxiety and real-world mood (Hur et al., 2020a), relations between threat-related brain activity and real-world mood dynamics (Hur et al., 2022), and the neuroanatomical correlates of early-life anxiety, shyness, and behavioral inhibition (Bas-Hoogendam et al., 2022) but have never been used to address the present aims.

Power analyses

The sample size was determined a priori as part of the application for the grant that supported data collection (R01-MH107444). The target sample size ($N \approx 240$) was chosen to afford acceptable power and precision given available resources. At the time of study design, G-power (version 3.1.9.2) indicated >99% power to detect a benchmark ("generic") medium-sized effect ($r = 0.30$) with up to 20% planned attrition ($N = 192$ usable datasets) using $\alpha = 0.05$, two-tailed (Erdfelder et al., 1996). The final sample of 220 usable fMRI datasets (see below) provides 80% power to detect a focal brain–temperament association as small as $r = 0.186$ ($R^2 = 3.46\%$).

Participants

A total of 241 participants were recruited and scanned. Of these, six withdrew due to excess distress in the scanner, one withdrew from the study

Table 1. Human studies of N/NE and distress-eliciting neuroimaging paradigms

Study	N (% male)	N/NE	MRI field strength (T)	EPI voxel size (mm³)	Normalization[a]	Trait-relevant challenge(s)	Analysis type	Summary of EAc results
Present study	220 (49.5%), stratified sampling to capture a broad spectrum of N/NE; screened to exclude current internalizing illness	Multiscale, multioccasion composite	3	10.5	BBR and diffeomorphic	Anticipation of uncertain/certain aversive shock, auditory clips, and photographs; negative emotional faces vs place scenes	ROIs, voxelwise	See the main report
Brinkmann et al. (2018)	93 (35.5%), screened to exclude any internalizing illness in the past 5 years	STAI	3	15.3	Affine and manual TT	Aversive photographs	NR	NS
Indovina et al. (2011)	23 (43.5%), screened to exclude lifetime internalizing illness	STAI	3	18.0	"SPM5"	Pavlovian threat cue (auditory UCS; uninstructed)	Amygdala ROI	Positive relations between the magnitude of amygdala reactivity and N/NE
Kirlic et al. (2019)	83 (42.2%), 43 of whom had depression or anxiety disorder diagnoses	Multiscale composite	3	18.1	"AFNI" and diffeomorphic	Anticipation of uncertain shock	Voxelwise	NS
Klumpers et al. (2017)	108 (100%), screened to exclude lifetime internalizing illness	STAI	1.5	38.1	"SPM8"	Anticipation of uncertain shock	Amygdala and BST ROIs	NS
Schuyler et al. (2012)	127 (36.2%), screened to exclude past-year internalizing illness	BFI-N	3	56.25	Affine	Aversive photographs	Amygdala fROI	Positive relations between the persistence of amygdala reactivity and N/NE
Sjouwerman et al. (2020)	113 (61.1%), screened to exclude lifetime internalizing illness	STAI	3	8.0	"SPM8"	Pavlovian threat cue (shock UCS; uninstructed)	Amygdala SVC	Positive relations between amygdala reactivity and N/NE
Somerville et al. (2010)	50 (44%), screened to exclude lifetime internalizing illness	Multiscale composite	3	31.5	"SPM2"	Anticipation of uncertain shock	Amygdala and BST fROIs, voxelwise	Positive relations between the magnitude of BST reactivity and N/NE; NS amygdala
Visser et al. (2021)	98 (30.6%), screened to exclude lifetime internalizing illness	STAI	3	8.0	BBR and diffeomorphic	Pavlovian threat cue (shock UCS; uninstructed)	Amygdala SVC	NS Amygdala

AFNI, Analysis of Functional NeuroImages software package; BBR, boundary-based registration of the T1- and T2-weighted images; BFI-N, Big Five Inventory–Neuroticism; EAc, central extended amygdala; fROI, functionally defined region of interest (all others are anatomically defined); NEO-FFI, neuroticism/extraversion/openness five-factor inventory-3; NR, not reported or indeterminate; NS, not significant; SPM#, Statistical Parametric Mapping software package (# indicates version); STAI, Spielberger state–trait anxiety inventory; SVC, small-volume corrected; TT, piecewise linear Talairach–Tournoux transformation; UCS, unconditioned stimulus.

[a]Older normalization techniques (e.g., affine) can introduce substantial spatial smoothing and registration error, which is a concern for work focused on small subcortical structures, such as the Ce and BST.

Recruitment and N/NE Phenotyping
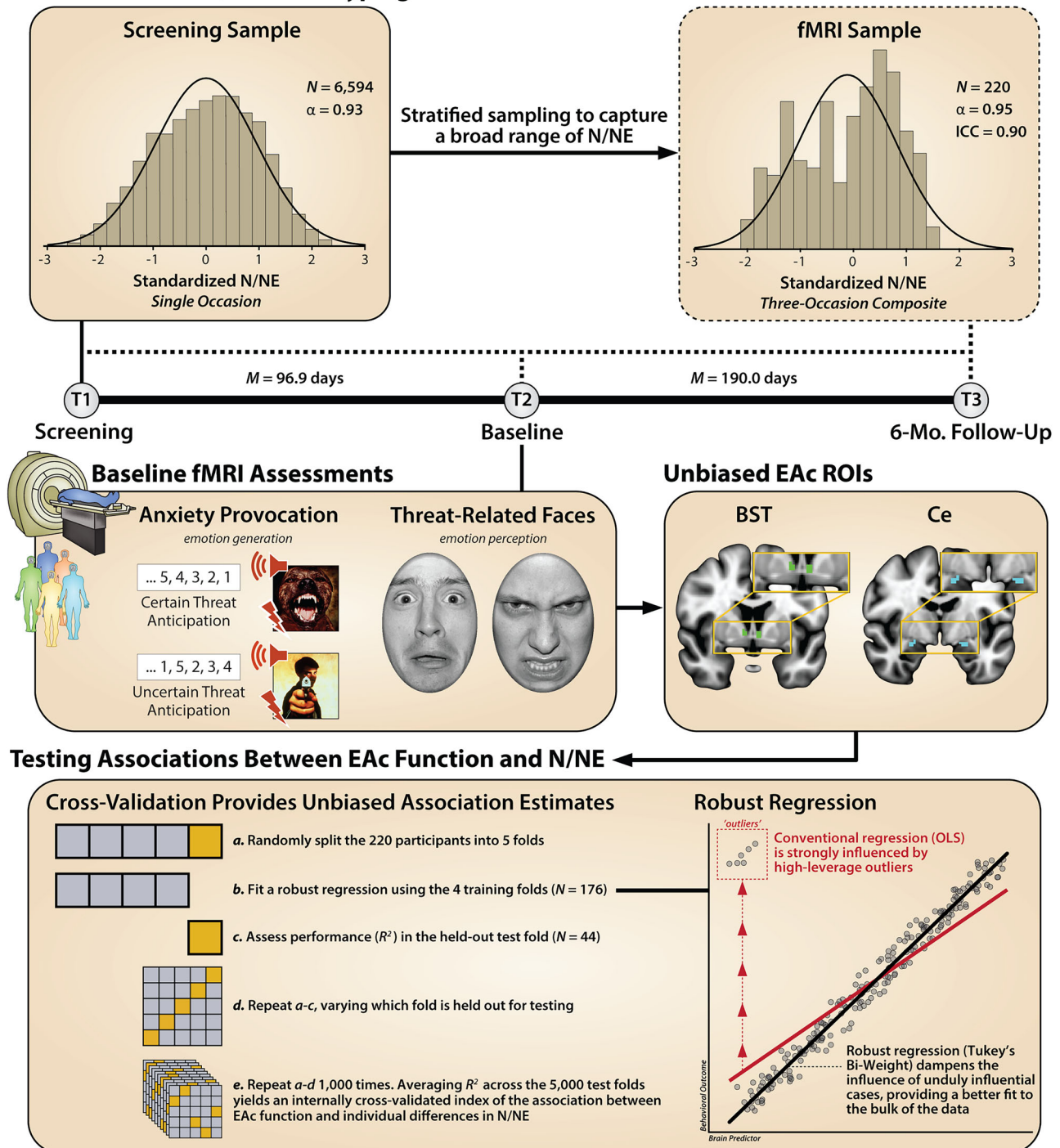
Figure 1. Study overview. Recruitment and N/NE phenotyping. To ensure a broad spectrum of N/NE, participants were selectively recruited from an ethnoracially diverse pool of 6,594 prescreened individuals. N/NE was assessed at screening (T1), at the baseline laboratory session (T2), and at the 6-month follow-up session (T3). To maximize reliability and power, analyses leveraged a composite measure of N/NE that was aggregated across two scales and three measurement occasions. Top panels indicate the distribution (histogram), internal-consistency reliability (α), and test–retest reliability of N/NE in the screening (left) and fMRI (right) samples. Timeline indicates the interval between assessments. Baseline fMRI assessments. Anxiety provocation. Following the baseline laboratory assessment (T2), participants completed an fMRI assessment. All participants completed the Maryland Threat Countdown paradigm, a well-established anxiety–provocation paradigm. The paradigm takes the form of a 2 (valence, threat/safety) × 2 (temporal certainty, certain/uncertain) factorial design. On threat trials, subjects saw a stream of integers that terminated with the temporally certain or uncertain presentation of a noxious electric shock, unpleasant photograph, and thematically related audio clip. Safety trials were similar but terminated with the delivery of benign stimuli. Hypothesis testing focused on neural activation associated with the anticipation of temporally certain and uncertain threat, relative to safety. A total of 220 individuals provided usable imaging data. Threat-related faces. An overlapping set of 213 participants also completed a "threat-related" (fearful/angry) faces fMRI paradigm. Participants viewed short blocks of photographs, alternating between blocks of faces and places (e.g., park, office). Hypothesis testing focused on activation associated with threat-related faces, relative to places. EAc ROIs. Anatomically defined ROIs enabled us to rigorously test the central hypothesis that N/NE reflects heightened recruitment of the BST (green) and potentially the Ce (dorsal amygdala; cyan), during the aversive anticipation of a genuinely aversive threat, and explore the possibility that these associations are more evident when the timing of threat encounters is uncertain. Unlike conventional whole-brain voxelwise analyses—which screen thousands of voxels for statistical significance and yield optimistically biased associations—anatomically defined ROIs "fix" the measurements of interest a priori, providing statistically unbiased estimates of brain–phenotype associations. Standardized regression coefficients were extracted and averaged
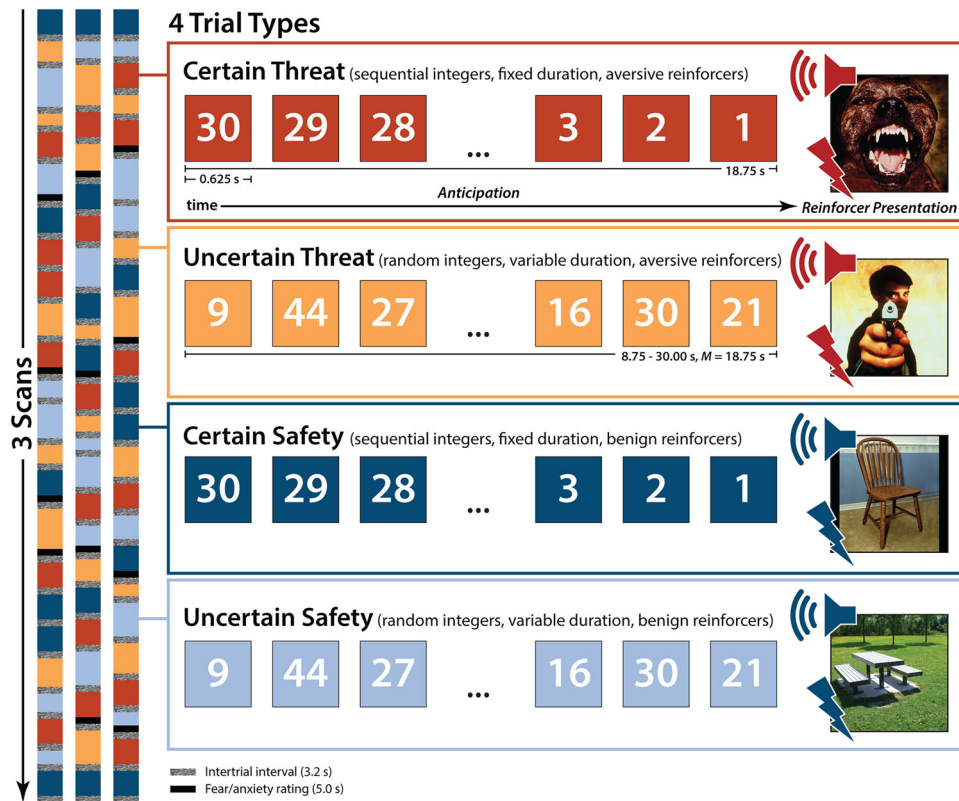
Figure 2. Threat-anticipation paradigm. The Maryland Threat Countdown paradigm takes the form of a 2 (valence, threat/safety) × 2 (temporal certainty: certain/uncertain) repeated-measure, randomized event-related design. Participants were completely informed about the task design and contingencies prior to scanning. The task was administered in three scans, with short breaks between scans. On certain-threat trials, participants saw a descending stream of integers ("countdown") for 18.75 s. To ensure robust distress, this anticipation epoch always terminated with the presentation of a noxious electric shock, unpleasant photograph, and thematically related audio clip (e.g., scream). Uncertain-threat trials were similar, but the integer stream was randomized and presented for an uncertain and variable duration (8.75–30.00 s; M = 18.75 s). Participants knew that something aversive was going to occur, but they had no way of knowing precisely when. Safety trials were similar but terminated with the delivery of benign reinforcers (e.g., just-perceptible electrical stimulation). White-noise visual masks (3.2 s) were presented between trials to minimize persistence of visual reinforcers in iconic memory. Participants were periodically prompted to rate the intensity of fear/anxiety experienced a few seconds earlier, during the anticipation ("countdown") epoch of the prior trial. Skin conductance was continuously acquired.

after the imaging session, and four were excluded due to incidental neurological findings.

Threat-anticipation paradigm. One participant was excluded from fMRI analyses due to gross susceptibility artifacts in the echoplanar imaging (EPI) data, 2 were excluded due to insufficient usable data (see below), 6 were excluded due to excess motion artifact (see below), and 1 was excluded due to task timing issues, yielding an ethnoracially diverse final sample of 220 participants (49.5% female; 61.4% White, 18.2% Asian, 8.6% African American, 4.1% Hispanic, 7.3% Multiracial/Other; M = 18.8 years; SD = 0.4). Of these, two participants were excluded from skin conductance analyses due to insufficient usable data (see below).

Threat-perception (emotional-faces) paradigm. Three participants were excluded due to gross susceptibility artifacts in the EPI data, 1 was excluded due to insufficient usable data (see below), 7 were excluded due to excessive motion artifact (see below), and 6 participants for

inadequate behavioral performance (see below), yielding a final sample of 213 participants (49.3% female; 61.0% White, 17.8% Asian, 8.5% African American, 4.2% Hispanic, 7.0% Multiracial/Other; M = 18.8 years; SD = 0.3). A subset of 209 participants (98.1%) provided usable data for both fMRI tasks and were used for the cross-task association analyses.

N/NE

Broadband N/NE. As in our prior work (Shackman et al., 2018; Hur et al., 2020a,b, 2022), we used well-established measures of neuroticism (Big Five Inventory-Neuroticism; John et al., 2008) and trait anxiety (International Personality Item Pool-Trait Anxiety; Goldberg, 1999; Goldberg et al., 2006) to quantify individual differences in N/NE on three occasions: screening, baseline, and 6 month follow-up (Fig. 1). Participants used a 1 (disagree strongly) to 5 (agree strongly) scale to rate a total of 18 items (e.g., depressed or blue, tense, worry, nervous, get distressed easily, fear for the worst, afraid of many things). At the screening, the neuroticism and anxiety scales were strongly correlated

←

across voxels for each combination of ROI, task contrast, and participant. Testing associations between EAc function and N/NE. Cross-validation provides statistically unbiased association estimates. Conventional-regression approaches use all available data for model fitting ("training"), yielding optimistically biased estimates of model performance (R^2) that do not generalize well to unseen data ("overfitting"). As shown in the bottom-left panel, we used a well-established cross-validation framework (i.e., repeated fivefold) to compute statistically unbiased associations. Robust regression. As shown in the bottom-right panel, conventional regression is sensitive to high-leverage outliers (red). Here we used robust regression (Tukey's biweight) to reduce the influence of unduly influential cases, providing a better fit to the bulk of the data and reducing volatility across the cross-validated training (N = 176) and test (N = 44) folds. The same analytic framework was used for the faces paradigm. a, Cronbach's alpha (internal-consistency reliability); BST, bed nucleus of the stria terminalis; Ce, dorsal amygdala in the region of the central nucleus; EAc, central extended amygdala; ICC, intraclass correlation (test–retest reliability); M, mean; Mo., months; N, number of observations; N/NE, neuroticism/negative emotionality; OLS, ordinary least squares; ROI, region of interest.

Robust Test-Retest Reliability
Substantial Rank-Order Variability
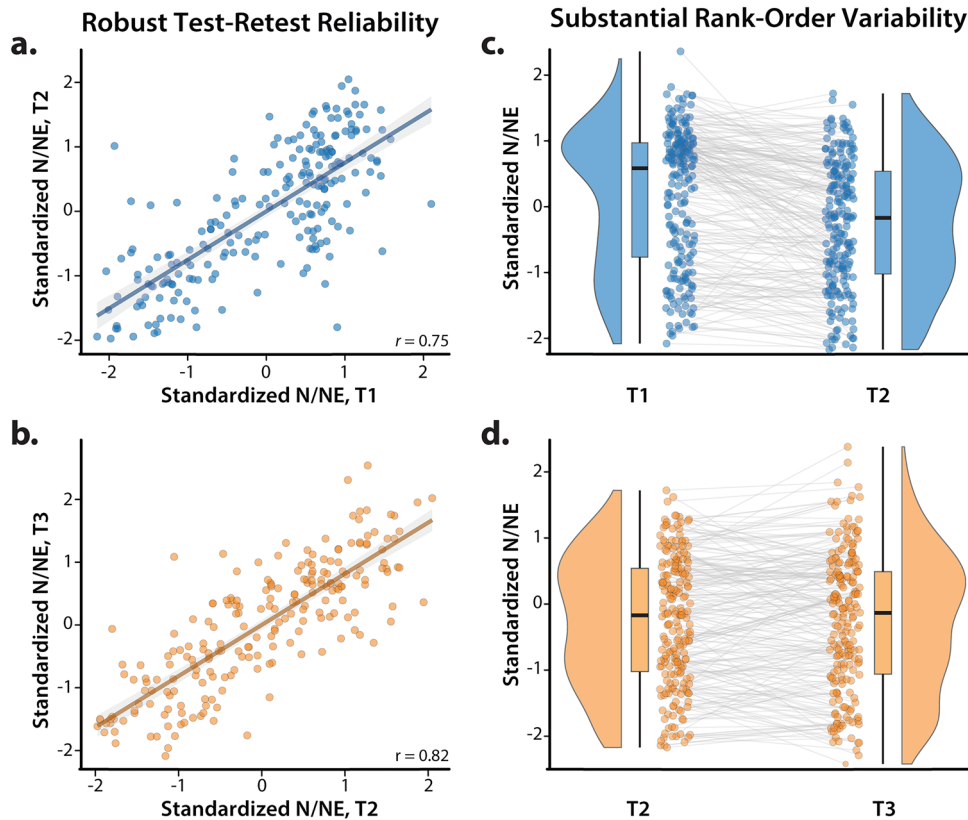
Figure 3. Robust test-retest reliability belies substantial rank-order variability in N/NE. A voluminous literature underscores the reliability of questionnaire measures of personality and temperament (Soto and John, 2017). Indeed, as shown in panels *a* and *b*, our multiscale measure of N/NE showed robust test–retest reliability across successive measurement occasions (compare Fig. 1). Nevertheless, inspection of the raincloud plots depicted in panels *c* and *d* revealed notable variability in the rank order of participants, with 46.4% of the sample showing at least a 0.5 SD change between T1 (screening) and T2 (baseline), 41.4% between T2 and T3 (6 month follow-up), and 55.9% between T1 and T3. In short, even highly reliable single-occasion measurements of N/NE contain considerable state and error variance (Roemer et al., in press). Consistent with recent methodological recommendations (Nikolaidis et al., 2022), we addressed this by creating a composite measure of N/NE that was aggregated across two scales and three measurement occasions (T1–T3), maximizing reliability and power to detect brain-temperament associations. Scatterplots depict standard (ordinary least squares) regression estimates. Gray bands indicate 95% confidence intervals. Raincloud plots depict the smoothed density distributions (i.e., "bean" or "half-violin") of standardized N/NE. Box-and-whisker plots indicate the medians (horizontal lines) and interquartile ranges (boxes). Whiskers depict 1.5 times the interquartile range. Colored dots connected by gray lines indicate changes in standardized N/NE for each participant.

(rs > 0.85) and internally consistent (αs > 0.85). To minimize the influence of short-term fluctuations in responding, hypothesis testing employed a multiscale, multioccasion composite measure of N/NE. This was computed by z-transforming the neuroticism and trait anxiety scales (using the mean and variance from the much larger screening sample) and then averaging across scales and measurement occasions. The resulting composite captured a sizable range of the N/NE spectrum and demonstrated strong internal-consistency ($\alpha = 0.95$) and test–retest (ICC$_{3,k} = 0.90$) reliability (compare Figs. 1, 3).

N/NE facets. Epidemiological, psychiatric, and biological studies typically focus on broadband measures of N/NE, such as the Eysenck personality questionnaire; Spielberger's state–trait anxiety inventory; and our own multiscale composite (see above; Shackman et al., 2016; Hur et al., 2019). Yet it is clear that N/NE is a complex phenotype that subsumes several narrower traits, including dispositional fear/anxiety, depression/sadness, and anger/irritability (Caspi et al., 2005; Soto and John, 2017). N/NE is also associated with elevated emotional volatility (Soto and John, 2017; Kalokerinos et al., 2020). Basic affective neuroscience research suggests that each of these facets of N/NE reflects partially distinct neural circuits, and recent research demonstrates a mixture of shared and unique psychological associations and biological substrates (Soto and John, 2017; Fox et al., 2018; Thorp et al., 2021; Klein-Flügge et al., 2022; Watson et al., 2022; Khoo et al., 2023). To understand which facets of N/NE are most closely associated with EAc reactivity, we leveraged the revised Big Five Inventory (BFI-2), a well-established, hierarchically organized scale that was purposely constructed to enable

psychometrically rigorous facet-level analyses (Soto and John, 2017). At the baseline and 6 month follow-up sessions (but not the screening assessment), participants used a 1 (disagree strongly) to 5 (agree strongly) scale to rate 12 items (four items/facet) indexing dispositional anxiety (e.g., anxious or afraid), depression/sadness (e.g., sad), and emotional volatility (e.g., easily upset, moody). Paralleling the approach used for broadband N/NE, facet scores were averaged across assessments to minimize occasion-specific fluctuations. All three facets demonstrated adequate internal-consistency ($\alpha = 0.81$–0.88) and test–retest ($r = 0.69$–0.79) reliability. As expected, all were robustly correlated with our broadband composite ($r = 0.74$–0.92). Interfacet associations, while substantial, indicated substantial unique variance ($r = 0.68$–0.71; $R^2 < 51\%$).

Threat-anticipation paradigm
Paradigm structure and design considerations. The Maryland Threat Countdown paradigm is an fMRI-optimized variant of temporally uncertain-threat assays that have been validated using fear-potentiated startle and acute anxiolytic administration (e.g., benzodiazepine) in mice, rats, and humans (Miles et al., 2011; Hefner et al., 2013; Daldrup et al., 2015; Lange et al., 2017; Moberg et al., 2017). The paradigm has been successfully deployed in a sample of university students that overlaps the sample featured here (Hur et al., 2020b, 2022) and in an independent sample of community volunteers (H. C. Kim et al., 2023).

As shown in Figure 2, the Maryland Threat Countdown takes the form of a 2 (valence, threat/safety) × 2 (temporal certainty, uncertain/certain) randomized, event-related, repeated-measure design (three scans; six trials/condition/scan). Subjects were completely informed
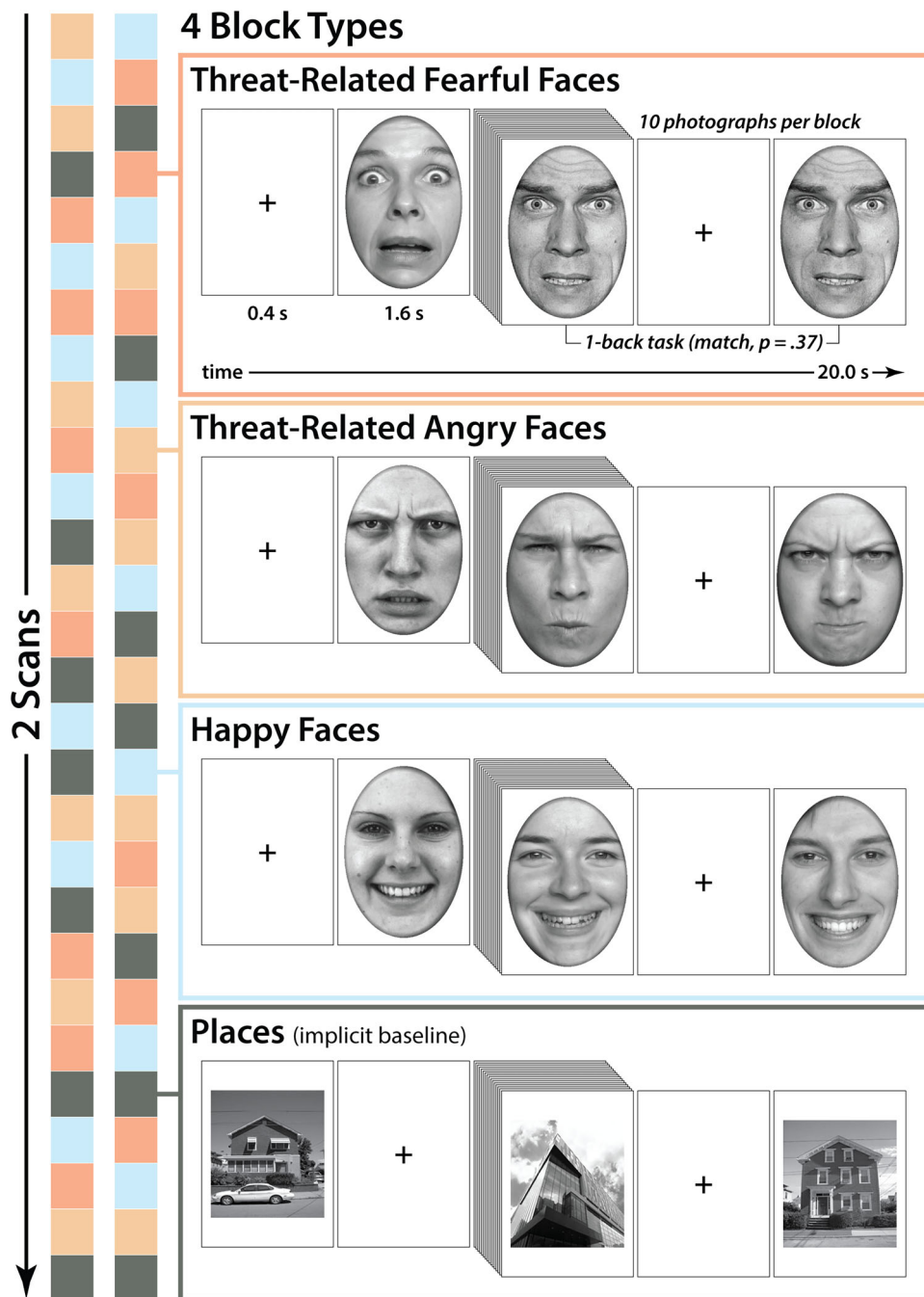
Figure 4. Threat-perception (emotional-faces) paradigm. The emotional-faces paradigm took the form of a pseudorandomized block design and was administered in two scans. During each scan, participants viewed standardized photographs of adults (half female) modeling prototypical angry faces, fearful faces, happy faces, or places (i.e., emotionally neutral everyday scenes; 7 blocks/condition/scan). Blocks consisted of 10 briefly presented photographs of faces or places (1.6 s) separated by fixation crosses (0.4 s). To minimize potential habituation, we presented each photograph a maximum of two times. To ensure engagement, on each trial, participants judged whether the current photograph matched that presented on the prior trial (i.e., performed a "one-back" continuous–performance task).

about the task design and contingencies prior to scanning. Simulations were used to optimize the detection and deconvolution of task-related hemodynamic signals. Stimulus presentation and ratings acquisition were controlled using *Presentation* (version 19.0, Neurobehavioral Systems).

On certain-threat trials, participants saw a descending stream of integers ("countdown," e.g., 30, 29, 28…3, 2, 1) for 18.75 s. To ensure robust distress, this anticipation epoch culminated with the presentation of a noxious electric shock, unpleasant photograph (e.g., mutilated body), and thematically related audio clip (e.g., scream, gunshot). Uncertain-threat trials were similar, but the integer stream was

randomized and presented for an uncertain and variable duration (8.75–30.00 s; $M = 18.75$ s). Participants knew that something aversive was going to occur, but they had no way of knowing precisely when. Consistent with methodological recommendations (Shackman and Fox, 2016), the average duration of the anticipation epoch was identical across conditions, ensuring an equal number of measurements (TRs/ condition). The specific mean duration was chosen to enhance detection of task-related differences in the blood oxygen level-dependent signal ("activation"; Henson, 2007) and to allow sufficient time for sustained responses to become evident. Safety trials were similar but terminated with the delivery of benign reinforcers (see below). Valence was

continuously signaled during the anticipation epoch ("countdown") by the background color of the display. Temporal certainty was signaled by the nature of the integer stream. Certain trials always began with the presentation of the number 30. On uncertain trials, integers were randomly drawn from a near-uniform distribution ranging from 1 to 45 to reinforce the impression that they could be much shorter or longer than certain trials and to minimize incidental temporal learning ("time-keeping"). To concretely demonstrate the variable duration of uncertain trials, during scanning, the first three trials featured short (8.75 s), medium (15.00 s), and long (28.75 s) anticipation epochs. To mitigate potential confusion and eliminate mnemonic demands, we presented a lowercase "c" or "u" at the lower edge of the display throughout the anticipatory epoch. White-noise visual masks (3.2 s) were presented between trials to minimize the persistence of visual reinforcers in iconic memory.

Participants were periodically prompted (following the offset of the white-noise visual mask) to rate the intensity of fear/anxiety experienced a few seconds earlier, during the anticipation ("countdown") period of the prior trial, using a 1 (minimal) to 4 (maximal) scale and an MRI-compatible response pad (MRA). Each condition was rated once per scan (16.7% trials). Premature ratings (<300 ms) were censored. All participants provided at least six usable ratings and rated each condition at least once. Skin conductance was continuously acquired throughout.

Procedures. Prior to scanning, participants practiced an abbreviated version of the paradigm (without electrical stimulation) until they indicated and staff confirmed understanding. Benign and aversive electrical stimulation levels were individually titrated. *Benign Stimulation.* Participants were asked whether they could "reliably detect" a 20 V stimulus and whether it was "at all unpleasant." If the subject could not detect the stimulus, the voltage was increased by 4 V and the process repeated. If the subject indicated that the stimulus was unpleasant, the voltage was reduced by 4 V, and the process was repeated. The final level chosen served as the benign electrical stimulation during the imaging assessment ($M = 21.06$ V; SD = 5.06). *Aversive Stimulation.* Participants received a 100 V stimulus and were asked whether it was "as unpleasant as you are willing to tolerate"—an instruction specifically chosen to maximize anxious distress and arousal. If the subject indicated that they were willing to tolerate more intense stimulation, the voltage was increased by 10 V, and the process repeated. If the subject indicated that the stimulus was too intense, the voltage was reduced by 5 V, and the process repeated. The final level chosen served as the aversive electrical stimulation during the imaging assessment ($M = 117.85$ V; SD = 26.10). The intensity of aversive stimulation was weakly and negatively associated with individual differences in N/NE ($r_{(218)} = -0.13$; $p = 0.05$). Following each scan, staff reassessed whether stimulation was sufficiently intense and increased the level as necessary.

Electrical stimuli. Electrical stimuli (100 ms; 2 ms pulses every 10 ms) were generated using an MRI-compatible constant–voltage stimulator system (STMEPM-MRI; Biopac Systems). Stimuli were delivered using MRI-compatible, disposable carbon electrodes (Biopac Systems) attached to the fourth and fifth digits of the nondominant hand.

Visual stimuli. A total of 72 aversive and benign photographs (1.8 s) were selected from the International Affective Picture System (for details, see Hur et al., 2020b). Visual stimuli were digitally back-projected (Powerlite Pro G5550, Epson America) onto a semiopaque screen mounted at the head-end of the scanner bore and viewed using a mirror mounted on the head coil.

Auditory stimuli. A total of 72 aversive and benign auditory stimuli (0.8 s) were adapted from open-access online sources. Auditory stimuli were delivered using an amplifier (PA-1 Whirlwind) with inline noise-reducing filters and ear buds (S14; Sensimetrics) fitted with noise-reducing ear plugs (Hearing Components).

Skin conductance. Skin conductance was continuously acquired during each scan using a Biopac system (MP-150; Biopac Systems). Skin conductance (250 Hz; 0.05 Hz high-pass) was measured using MRI-compatible disposable electrodes (EL507) attached to the second and third digits of the nondominant hand.

Threat-perception (emotional-faces) paradigm
The emotional-faces paradigm took the form of a pseudorandomized block design and was administered in two scans, with a short break between scans (Fig. 4). During each scan, participants viewed standardized photographs of adults (half female) modeling prototypical angry faces, fearful faces, happy faces, or places (i.e., emotionally neutral everyday scenes; seven blocks/condition/scan). To maximize signal strength and homogeneity and mitigate potential habituation (Henson, 2007; Maus et al., 2010; Plichta et al., 2014), each 20 s block consisted of 10 briefly presented photographs of faces or places (1.6 s) separated by fixation crosses (0.4 s). To minimize potential habituation, each photograph was presented a maximum of two times (for details, see Hur et al., 2020b). To ensure engagement, on each trial, participants judged whether the current photograph matched that presented on the prior trial (i.e., a "one-back" continuous–performance task). Matches occurred 37.1% of the time.

MRI data acquisition
MRI data were acquired using a Siemens Magnetom TIM Trio 3 Tesla scanner (32-channel head coil). During scanning, foam inserts were used to immobilize the participant's head within the head coil and mitigate potential motion artifact. Participants were continuously monitored using an MRI-compatible eye tracker (EyeLink 1000; SR Research) and the AFNI real-time motion plugin (Cox, 1996). Sagittal T1-weighted anatomical images were acquired using a magnetization-prepared rapid acquisition gradient echo sequence (TR, 2,400 ms; TE, 2.01 ms; inversion time, 1,060 ms; flip, 8°; slice thickness, 0.8 mm; in-plane, 0.8×0.8 mm; matrix, 300×320; field-of-view, 240×256). A T2-weighted image was collected coplanar to the T1-weighted image (TR, 3,200 ms; TE, 564 ms; flip angle, 120°). To enhance resolution, a multiband sequence was used to collect oblique-axial EPI volumes (multiband acceleration, 6; TR, 1,250 ms; TE, 39.4 ms; flip, 36.4°; slice thickness, 2.2 mm; number of slices, 60; in-plane resolution, 2.1875×2.1875 mm; matrix, 96×96). Images were collected in the oblique-axial plane ($\sim-20°$ relative to the AC-PC plane) to minimize potential susceptibility artifacts. For the threat-anticipation task, three 478-volume EPI scans were acquired. For the threat-perception (emotional-faces) task, two 454-volume EPI scans were acquired. The scanner automatically discarded seven volumes prior to the first recorded volume. To enable fieldmap correction, two oblique-axial spin echo (SE) images were collected in opposing phase-encoding directions (rostral-to-caudal and caudal-to-rostral) at the same location and resolution as the functional volumes (i.e., coplanar; TR, 7,220 ms; TE, 73 ms). Measures of respiration and pulse were continuously acquired during scanning using a respiration belt and photoplethysmograph affixed to the first digit of the nondominant hand. Following the last scan, participants were removed from the scanner, debriefed, compensated, and discharged.

Skin conductance data processing pipeline
Skin conductance data were processed using *PsPM* (version 4.0.2) and in-house MATLAB (version 9.9.0.1467703) code (Bach and Friston, 2013; Bach et al., 2018). Data were orthogonalized with respect to pulse and respiration signals and despiked using *filloutliers* (150-sample moving–median widow; modified Akima cubic Hermite interpolation). Each scan was then bandpass filtered (0.009–0.333 Hz), median centered, and downsampled (4 Hz). Subject-specific skin conductance response functions (SCRFs) were estimated by fitting the four parameters of the canonical SCRF (Bach et al., 2010) to the grand-average reinforcer response using *fmincon*, and a cost function that maximized variance explained and penalized negative coefficients.

MRI data processing pipeline
Methods were optimized to minimize spatial normalization error and other potential sources of noise. Data were visually inspected before and after processing for quality assurance.

Anatomical data processing. Methods are similar to those described in other recent reports by our group (Hur et al., 2020b, 2022; H. C. Kim et al., 2023). T1-weighted images were inhomogeneity corrected using *N4* (Tustison et al., 2010) and denoised using *ANTS* (Avants et al., 2011). The brain was then extracted using a combination of *BEaST* (Eskildsen et al., 2012) and brain-extracted-and-normalized reference brains (BIAC, 2022). Brain-extracted T1 images were normalized to a version of the brain-extracted 1 mm T1-weighted MNI152 (version 6) template (Grabner et al., 2006) modified to remove the extracerebral tissue. Normalization was performed using the diffeomorphic approach implemented in *SyN* (version 2.3.4; Avants et al., 2011). T2-weighted images were rigidly coregistered with the corresponding T1 prior to normalization. The brain-extraction mask from the T1 was then applied. Tissue priors were unwarped to native space using the inverse of the diffeomorphic transformation (Lorio et al., 2016). Brain-extracted T1 and T2 images were segmented—using native-space priors generated in *FAST* (version 6.0.4; Jenkinson et al., 2012)—for subsequent use in T1-EPI coregistration (see below).

Fieldmap data processing. SE images and *topup* were used to create fieldmaps. Fieldmaps were converted to radians, median-filtered, and smoothed (2 mm). The average of the distortion-corrected SE images was inhomogeneity corrected using *N4* and masked to remove extracerebral voxels using *3dSkullStrip* (version 19.1.00).

Functional data processing. EPI files were despiked using *3dDespike*, slice time-corrected to the TR center using *3dTshift*, and motion-corrected to the first volume and inhomogeneity corrected using *ANTS* (12-parameter affine). Transformations were saved in an ITK-compatible format for subsequent use (McCormick et al., 2014). The first volume was extracted for EPI-T1 coregistration. The reference EPI volume was simultaneously coregistered with the corresponding T1-weighted image in native space and corrected for geometric distortions using boundary-based registration (Jenkinson et al., 2012). This step incorporated the previously created fieldmap, undistorted SE, T1, white matter (WM) image, and masks. To minimize incidental spatial blurring, the spatial transformations necessary to transform each EPI volume from native space to the reference EPI, from the reference EPI to the T1, and from the T1 to the template were concatenated and applied to the processed EPI data in a single step. Normalized EPI data were resampled (2 mm^3) using fifth-order B-splines. Hypothesis testing focused on anatomically defined EAc ROIs, as detailed below. To maximize anatomical resolution, no additional spatial filters were applied, consistent with prior work by our team and recent recommendations (Tillman et al., 2018; H. C. Kim et al., 2023).

Skin conductance data exclusions and modeling

Data exclusions. To ensure data validity, "scans" (i.e., runs) that did not show numerically positive skin conductance responses to reinforcer (e.g., shock) presentation (averaged across trials) were censored. Participants with <2 usable scans were excluded from skin conductance analyses (see above).

First-level modeling. Robust general linear models (GLMs) were used to separate electrodermal signals associated with the threat-anticipation ("countdown") epochs from those evoked by other aspects of the task (e.g., reinforcer delivery). Modeling was performed separately for each participant and scan using *robustfit*. Subject-specific SCRFs were convolved with rectangular regressors time-locked to the presentation of the reinforcers (separately for each trial type), visual masks, and rating prompts. To quantify the skin conductance level (SCL) during the anticipation epochs, first-level residuals were averaged separately for each participant and condition.

fMRI data exclusions, modeling, and derivative variables

Data exclusions. Volume-to-volume displacement (>0.5 mm) was used to assess residual motion artifact. Scans with excessively frequent artifacts (>2 SD) were discarded. Participants with insufficient usable fMRI data (<2 scans of the threat-anticipation task or <1 scan of the threat-perception task) or who showed poor behavioral performance

on the threat-perception task (see above; accuracy <2 SD) were excluded from the relevant analyses (see above).

First-level (single-subject) fMRI modeling. For each participant, first-level modeling was performed using GLMs implemented in *SPM12* (version 7771), with the default autoregressive model and the temporal bandpass filter set to the hemodynamic response function (HRF) and 128 s (Wellcome Centre for Human Neuroimaging, 2022). Regressors were convolved with a canonical HRF. *Threat-Anticipation Paradigm.* Hemodynamic reactivity was modeled using variable-duration rectangular ("boxcar") regressors that spanned the entirety of the anticipation ("countdown") epochs of uncertain-threat, certain-threat, and uncertain-safety trials. To maximize design efficiency, certain-safety anticipation served as the reference condition and contributed to the baseline estimate (Poline et al., 2007). Epochs corresponding to the presentation of the four types of reinforcers, white-noise visual masks, and rating prompts were simultaneously modeled using the same approach. EPI volumes acquired before the first trial and following the final trial were unmodeled and contributed to the baseline estimate. Consistent with prior work (Hur et al., 2020b, 2022; H. C. Kim et al., 2023), nuisance variates included estimates of volume-to-volume displacement, motion (6 parameters × 3 lags), cerebrospinal fluid (CSF) signal, instantaneous pulse and respiration rates, and ICA-derived nuisance signals (e.g., brain edge, CSF edge, global motion, WM; Pruim et al., 2015). Volumes with excessive volume-to-volume displacement (>0.5 mm) and those during and immediately following reinforcer delivery were censored. *Threat-Perception (Emotional-Faces) Paradigm.* Hemodynamic reactivity to blocks of each emotional expression (angry, fearful, and happy) was modeled using time-locked rectangular regressors. Place blocks served as the reference condition and contributed to the baseline estimate (Poline et al., 2007).

EAc ROIs. Consistent with prior work by our group, task-related Ce and BST activation was quantified using well-established, anatomically defined ROIs and spatially unsmoothed fMRI data (Tillman et al., 2018; H. C. Kim et al., 2023; compare Fig. 1). The derivation of the Ce ROI is detailed in Tillman et al. (2018). The probabilistic BST ROI was developed by Theiss and colleagues and thresholded at 25% (Theiss et al., 2017). It mostly encompasses the supracommissural BST, given the difficulty of reliably discriminating the borders of regions below the anterior commissure in T1-weighted images (Kruger et al., 2015). Bilateral ROIs were decimated to the 2 mm resolution of the fMRI data. EAc ROI analyses used standardized regression coefficients extracted and averaged for each contrast (e.g., uncertain-threat anticipation), region, and participant. Unlike conventional whole-brain voxelwise analyses—which screen thousands of voxels for statistical significance and yield optimistically biased associations—anatomically defined ROIs "fix" the measurements of interest a priori, providing statistically unbiased estimates of brain–phenotype associations (Poldrack et al., 2017).

Analytic strategy

Overview. Analyses were performed using a combination of *SPM12* (Wellcome Centre for Human Neuroimaging, 2022), *R* (version 4.0.2), *Rstudio* (version 1.2.1335), *JASP* (version 0.17.1), and *jamovi* (version 2.3.16; Love et al., 2019; R Core Team, 2022; RStudio Team, 2022; The jamovi project, 2023). Some analyses were performed using *psych* (version 2.2.5; Revelle, 2022) and *stats* (version 4_4.0.2; R Core Team, 2022). Diagnostic procedures and data visualizations were used to confirm that test assumptions were satisfied (Tukey, 1977). Some figures were created using *ggplot2* (version 3.3.6; Wickham, 2016), *raincloudplots* (version 0.2.0; Allen et al., 2021), and *MRIcron* (Rorden, 2019). Clusters and peaks were labeled using the Harvard–Oxford Atlas (Frazier et al., 2005; Desikan et al., 2006; Makris et al., 2006).

Confirmatory testing. As a precursor to hypothesis testing, we used standard repeated-measure GLMs to confirm that the threat-anticipation paradigm amplified subjective symptoms of distress (in-scanner fear/anxiety ratings) and objective signs of arousal (SCL). These analyses also afforded an opportunity to explore whether individual differences in N/NE amplify reactivity to a well-controlled, genuinely distressing experimental challenge (Maryland Threat Countdown; Shackman et al., 2016).

Using the multiscale, multioccasion composite (see above), mean-centered N/NE was included as a fully crossed dimensional covariate. Significant interactions were decomposed using focal contrasts and regressions. Exploratory nonparametric tests yielded similar conclusions (not reported).

We also confirmed that the threat-anticipation paradigm recruited the EAc. To maximize reliability, we focused on estimates of activation (e.g., uncertain-threat anticipation) relative to the implicit baseline (certain-safety anticipation; Brown et al., 2011; Infantolino et al., 2018; Baranger et al., 2021; Heilicher et al., 2022; Kennedy et al., 2022). Spatially unsmoothed data and whole-brain voxelwise ("second-level") repeated-measure GLMs ("random effects") were used to separately examine certain and uncertain threat (vs implicit baseline). We also examined the broader contrast of threat relative to safety anticipation. Significance was assessed using FDR $q < 0.05$ (whole-brain corrected). A series of one-sample Student's t tests was used to confirm that the anatomically defined EAc ROIs (BST and Ce) showed nominally significant activation during certain- and uncertain-threat anticipation ($p < 0.05$, uncorrected). A standard 2 (region: BST, Ce) × 2 (certainty: certain, uncertain) repeated-measure GLM was used to explore potential regional differences in sensitivity to certain-versus-uncertain threat anticipation. The same general approach was used to confirm that threat-related faces (vs implicit baseline) recruit the EAc (BST and Ce). Whole-brain statistical parametric maps are freely available at Neurovault.org (https://neurovault.org/collections/13109). Processed ROI data are freely available at the Open Science Framework (https://osf.io/w5cdk).

Hypothesis testing and exploratory analyses. The primary aim of the present study was to test the hypothesis that variation in N/NE is associated with heightened recruitment of the BST and potentially the Ce, during the anticipation of threat, and determine whether this association is more evident when the timing of threat encounters is uncertain. Two robust-regression models were implemented for each ROI (BST and Ce). The first quantified relations between individual differences in N/NE—indexed using the multiscale, multioccasion composite—and general threat reactivity, independent of the temporal certainty of aversive stimulation (threat vs safety anticipation). The second model quantified relations between N/NE and uncertain-threat reactivity, controlling for certain-threat reactivity. This provides an estimate of the variance in N/NE uniquely explained by BST or Ce activation during the anticipation of temporally uncertain (and/or certain) threat.

Conventional-regression approaches use all available data for model testing, yielding optimistically biased estimates of performance (R^2) that do not generalize well to unseen data (model "overfitting"; Marek et al., 2022; Spisak et al., 2023). To address this, we used k-folds cross-validation (fivefold × 1,000 repetitions) to compute statistically unbiased estimates of brain–temperament associations (cross-validated R^2; Poldrack et al., 2020). Conventional regression is also sensitive to stochastic noise (e.g., sampling and measurement error). This can be conceptualized as another form of model overfitting. Estimates derived from such models can change dramatically given relatively small changes in the data, rendering them intrinsically less reproducible (Yarkoni and Westfall, 2017; Yu and Yao, 2017). Here we instead used a robust-regression approach (Tukey's biweight), which reduces the impact of unduly influential cases, provides a better fit to the bulk of the data, and reduces volatility across the cross-validated training ($N = 176$) and test ($N = 44$) folds (Fig. 1; Yu and Yao, 2017). Robust- and conventional-regression approaches show similar performance when conventional-model assumptions are met (Kafadar, 1983; Wager et al., 2005; Yu and Yao, 2017).

Hypothesis testing was implemented using *caret* (version 6.0-86) and the default Tukey's biweight loss function ($c = 4.685$), which provides 95% asymptotic efficiency when conventional-regression assumptions are satisfied (Kafadar, 1983; Kuhn et al., 2020). By convention, final models were trained using all available data. To clarify specificity, we used the same analytic framework to quantify relations between N/NE and EAc reactivity to threat-related faces. Conventional-regression results are available at the Open Science Framework (https://osf.io/w5cdk). Sensitivity analyses confirmed that our key conclusions remained unchanged when controlling for potential nuisance variation in the mean-centered intensity of self-selected aversive electrical stimulation (not reported).

When significant associations between EAc threat reactivity and N/NE were detected, follow-up analyses were used to compare the strength of association across brain metrics (Hotelling, 1940) and explore potential associations with individual differences in the intensity of task-elicited distress (mean-centered fear/anxiety ratings). We also explored the relevance of narrower emotional traits, indexed using the mean-centered BFI-2 anxiety, depression/sadness, and emotional volatility facet scales (averaged across the baseline and 6 month follow-up assessments). Separate robust GLMs were computed for each facet scale.

Whole-brain voxelwise GLMs (random effects) were used to explore associations between mean-centered N/NE and activation in less intensely scrutinized regions. No significant voxelwise associations were detected (FDR $q < 0.05$, corrected).

The second aim of the present study was to determine whether threat-anticipation and threat-perception are interchangeable probes of individual differences in EAc function, that is, whether the two fMRI paradigms show "convergent validity" (Villalta-Gil et al., 2017). Using the same analytic framework detailed above, we computed robust between-task correlations, separately for the BST and Ce ROIs, for each of the key imaging contrasts. Demonstrating that individual differences in BST and/or Ce activation during the anticipation of threat (aversive multimodal stimulation) are strongly correlated with individual differences in activation during the presentation of threat-related (angry/fearful) faces would provide evidence of cross-task convergence.

Preregistration and deviation
Our general approach and hypotheses were preregistered (https://osf.io/wzhdm; Grogans and Shackman, 2021). The preregistration called for a conventional-regression approach. To enhance rigor, we adopted a cross-validated robust–regression framework for hypothesis testing. Recent work underscores the utility of cross-validation for reproducible estimates of brain–phenotype associations (Spisak et al., 2023).

Results

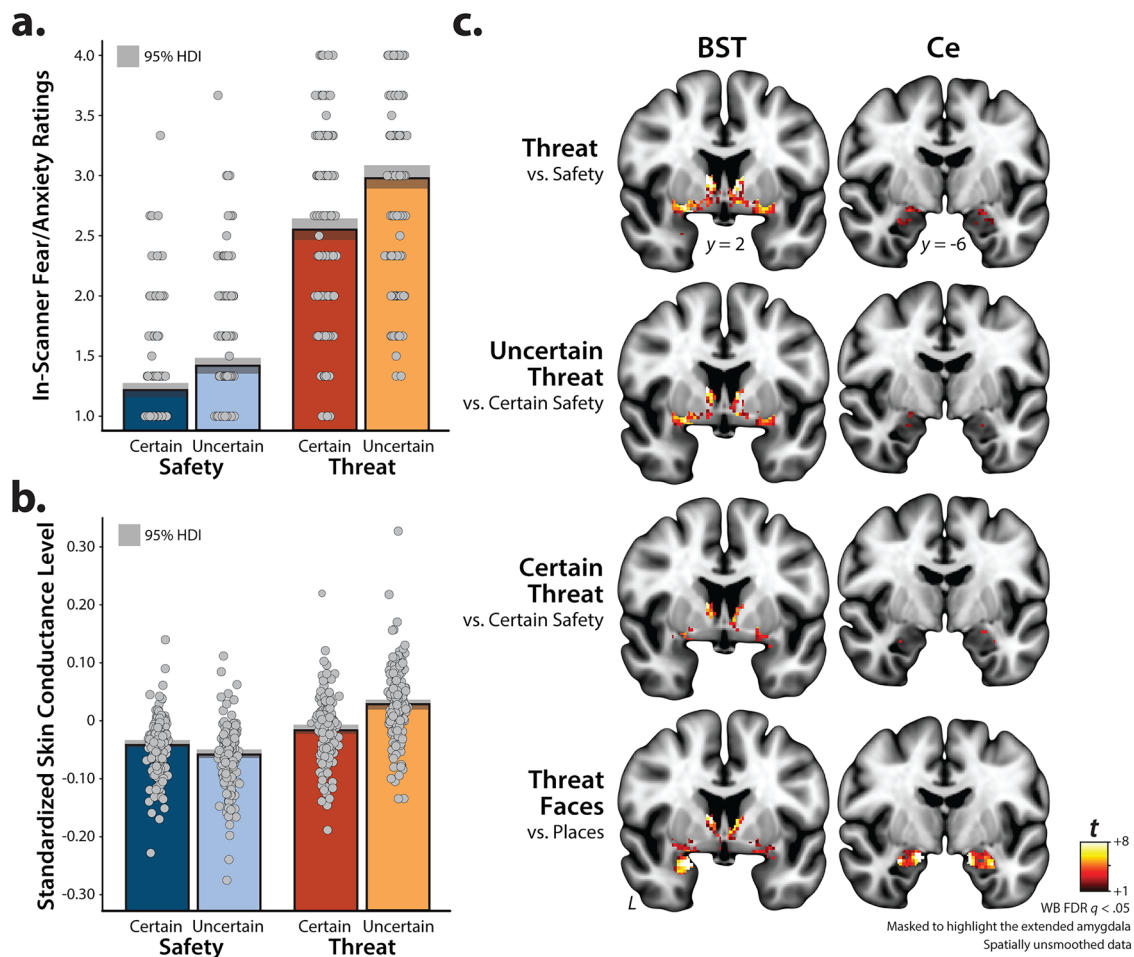### Threat anticipation amplifies subjective distress and objective arousal
We used standard repeated-measure GLMs to confirm that the threat-anticipation paradigm had the intended impact on anxious distress and arousal. Mean-centered N/NE was included as a fully crossed dimensional covariate, allowing us to explore the possibility that variation in N/NE influences reactivity to this well-controlled emotional challenge (Shackman et al., 2016).

As shown in Figure 5a, fearful and anxious feelings were significantly elevated during the anticipation of threat compared with that of safety, and this was particularly evident when the timing of threat encounters was uncertain (valence, $F_{(1,218)} = 1,135.06$; $p < 0.001$; certainty, $F_{(1,218)} = 212.95$; $p < 0.001$; valence × certainty, $F_{(1,218)} = 31.75$; $p < 0.001$; threat, uncertain vs certain, $F_{(1,218)} = 148.90$; $p < 0.001$; safety, uncertain vs certain, $F_{(1,218)} = 78.78$; $p < 0.001$).

As shown in Figure 5b, the same general pattern was evident for skin conductance, an objective psychophysiological index of arousal (valence, $F_{(1,216)} = 790.55$; $p < 0.001$; certainty, $F_{(1,216)} = 138.95$; $p < 0.001$; valence × certainty, $F_{(1,216)} = 661.63$; $p < 0.001$; threat, uncertain vs certain, $F_{(1,216)} = 455.78$; $p < 0.001$; safety, uncertain vs certain, $F_{(1,216)} = 270.03$; $p < 0.001$). These observations confirm the validity of the threat-anticipation paradigm as an experimental probe of fear and anxiety, consistent with prior work (Hur et al., 2020b, 2022; Chavanne and Robinson, 2021; H. C. Kim et al., 2023).

N/NE amplifies distress evoked by the threat-anticipation paradigm
Exploratory analyses demonstrated that individuals with a more negative disposition experienced pervasively elevated distress across the four conditions of the threat-anticipation

Figure 5. The threat-anticipation and threat-perception tasks are valid probes of EAc function. *a*, Threat anticipation evokes subjective distress. Fear and anxiety were increased during the anticipation of threat compared with that of safety, and this was particularly evident for temporally uncertain threat ($p < 0.001$). *b*, Threat anticipation evokes objective signs of arousal. A similar pattern was evident for skin conductance level ($p < 0.001$). *c*, Threat-anticipation and threat-perception recruit the EAc. As shown in the top three rows, the anticipation of threat, uncertain threat, and certain threat recruited the BST and the dorsal amygdala in the region of the Ce, when compared with their respective reference conditions ($q < 0.05$, corrected). As shown in the bottom row, the acute presentation of threat-related faces was also associated with significant activation in the region of the BST and the dorsal amygdala (Ce), relative to the reference condition. For additional details, see Extended Data Tables 5-1–5-4 (https://osf.io/w5cdk). Bars indicate the means (colored bars), Bayesian 95% highest density intervals (gray bands), and individual participants (gray dots). BST, bed nucleus of the stria terminalis; Ce, dorsal amygdala in the region of the central nucleus; FDR, false discovery rate; HDI, highest density interval; *t*, Student's *t*; WB, whole-brain corrected.

paradigm—both aversive and benign ($F_{(1,218)} = 33.57$; $p < 0.001$)—and modestly potentiated reactivity to the anticipation of threat compared with that of safety and to the anticipation of uncertain compared with that of certain outcomes (N/NE × valence, $F_{(1,218)} = 6.38$; $p = 0.01$; N/NE × certainty, $F_{(1,218)} = 6.03$; $p = 0.02$; Fig. 6). No other moderator effects were significant for either subjective distress or objective arousal ($p > 0.57$). In short, individuals with a more negative disposition show a mixture of indiscriminately elevated ("overgeneralized"), threat-potentiated, and uncertainty-potentiated anticipatory distress, in broad accord with prior work (Grupe and Nitschke, 2013; Shackman et al., 2016).

Threat anticipation and threat perception robustly recruit the EAc
We used standard whole-brain voxelwise GLMs to confirm that the threat-anticipation and threat-perception (emotional-faces) paradigms had the intended consequences on brain function. As expected, the anticipation of threat, uncertain threat, and certain threat significantly recruited both the BST and the dorsal amygdala in the region of the Ce (FDR $q < 0.05$, whole-brain corrected; Fig. 5c). Beyond the EAc, each of these contrasts was associated with

significant activation across a widely distributed network of regions previously implicated in the expression and regulation of human fear and anxiety (Shackman and Fox, 2021), including the midcingulate cortex, anterior insula/frontal operculum, dorsolateral prefrontal cortex, and periaqueductal gray (Extended Data Tables 5-1–5-3; https://osf.io/w5cdk). Analyses focused on the acute presentation of threat-related faces revealed significant activation in the region of the BST and the dorsal amygdala, consistent with prior work (Fig. 5c; Extended Data Table 5-4; https://osf.io/w5cdk; Fox and Shackman, 2019). Together, these observations demonstrate that our neuroimaging approach provides a robust probe of EAc function.

BST and Ce are similarly sensitive to certain-versus-uncertain threat anticipation
As a precursor to hypothesis testing, we used a series of *t* tests to confirm that the anatomically defined BST and Ce ROIs are recruited by the threat-anticipation and threat-perception (emotional-faces) tasks. Consistent with the voxelwise results (Fig. 5c), both ROIs did, in fact, show nominally significant activation ($ts_{(219)} > 3.10$; $ps < 0.002$, uncorrected; Fig. 7). A standard 2
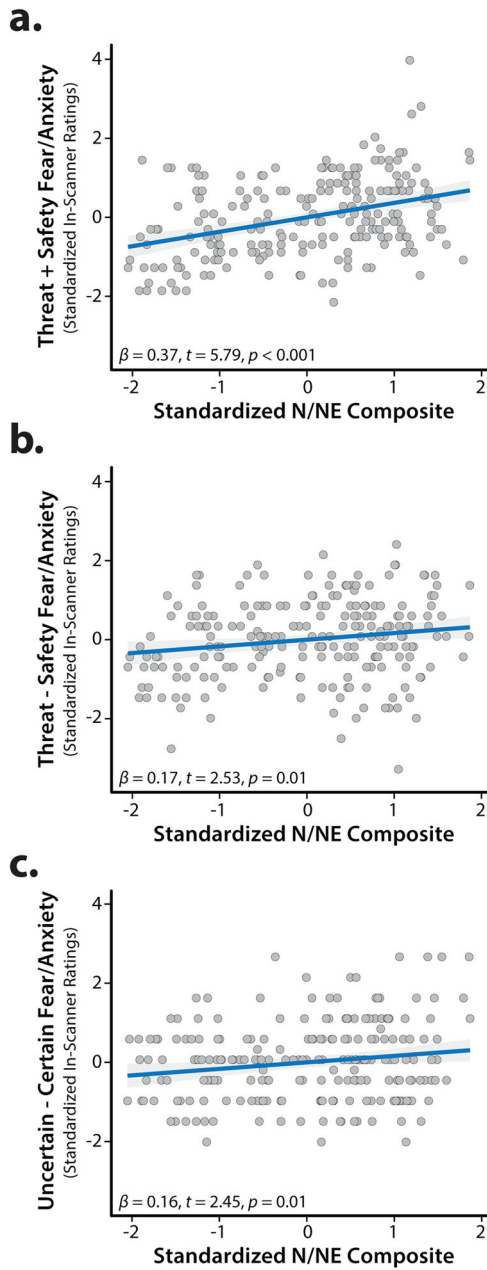
Figure 6. N/NE amplifies subjective fear and anxiety elicited by the threat-anticipation paradigm. Individuals with a more negative disposition showed a mixture of (*a*) indiscriminately elevated ("overgeneralized") distress across threat and safety trials, (*b*) potentiated distress when anticipating threat relative to safety, and (*c*) potentiated distress when anticipating temporally uncertain reinforcers. Scatterplots depict standard (ordinary least squares) regression estimates. Gray bands indicate 95% confidence intervals. N/NE, neuroticism/negative emotionality.

Figure 7. EAc ROI reactivity. The anatomically defined Ce and BST ROIs showed nominally significant activation during the (*a*) anticipation of threat and (*b*) presentation of threat-related faces (*ps* < 0.003). Relative to the Ce, the BST was more strongly recruited during periods of threat anticipation (*p* = 0.002). Neither the main effect of certainty nor the region × certainty interaction was significant (*p* > 0.18). Likewise, the direct contrast of certain-versus-uncertain threat was not significant in either ROI (*p* > 0.40). For additional details, see Extended Data Tables 7-1 and 7-2 (https://osf.io/w5cdk). Bars depict mean standardized ROI activation relative to the respective baseline conditions for each ROI (spatially unsmoothed data). Whiskers depict standard errors. Inset panels depict individual participants (gray dots). BST, bed nucleus of the stria terminalis ROI; Ce, central nucleus of the amygdala ROI; ROI, region of interest.

(region: BST, Ce) × 2 (certainty: certain, uncertain) GLM was used to explore potential regional differences in sensitivity to threat certainty. As shown in Figure 7a and detailed in Extended Data Tables 7-1 and 7-2 (https://osf.io/w5cdk), although the BST was more strongly activated, on average, by anticipated threat (region, $F_{(1,219)} = 9.36$; $p = 0.002$), neither the main effect of certainty nor the region × certainty ("double-dissociation") interaction was significant (certainty, $F_{(1,219)} = 0.19$; $p = 0.66$; region × certainty, $F_{(1,219)} = 0.85$; $p = 0.36$). Similarly, the direct contrast of the two threat-anticipation conditions was not significant in either region (BST, $t_{(219)} = -0.82$; $p = 0.41$; Ce, $t_{(219)} = 0.36$; $p = 0.72$). Collectively, these observations indicate the BST and Ce are

similarly sensitive to temporally certain and uncertain threat, extending prior work by our group (Hur et al., 2020b).

N/NE is associated with heightened BST activation during uncertain-threat anticipation

As shown schematically in Figure 1, cross-validated robust regressions were used to test the hypothesis that individuals with a more negative disposition will show exaggerated

recruitment of the EAc (BST and/or Ce) during threat anticipation and determine whether this association is more evident when the timing of threat encounters is uncertain. Results revealed that general EAc threat reactivity—aggregating across the anticipation of certain and uncertain aversive stimulation—was unrelated to individual differences in N/NE (BST, $\beta = 0.12$; $t_{(218)} = 1.57$; $p = 0.12$; Ce, $\beta = 0.02$; $t_{(218)} = 0.32$; $p = 0.75$; Fig. 8a,b). Prior work suggests that relations between N/NE and EAc function may be magnified when threat encounters are uncertain in their timing or likelihood (Somerville et al., 2010). To test this, we computed robust regressions between N/NE and EAc reactivity to uncertain threat, separately for each EAc region. To clarify specificity, models controlled for activation during certain-threat anticipation. Results demonstrated that heightened BST activation during uncertain-threat anticipation was significantly and selectively associated with trait-like variation in N/NE (uncertain, $\beta = 0.24$; $t_{(217)} = 2.61$; $p = 0.01$; certain, $\beta = -0.09$; $t_{(217)} = -1.00$; $p = 0.32$; Fig. 8c,d). Follow-up analyses indicated that this association was significantly stronger for uncertain threat ($t_{\text{Hotelling}(217)} = 2.42$; $p = 0.02$). Leveraging a simpler bivariate model, we estimated that BST reactivity to uncertain-threat anticipation explained, on average, 5.1% of the variance in N/NE in out-of-sample test folds ($\beta = 0.19$; $t_{(218)} = 2.59$; $p = 0.01$; cross-validated $R^2 = 0.051$). BST reactivity was unrelated to individual differences in task-related distress ($|t| < 1.00$; $p > 0.31$).

In contrast to the BST, Ce reactivity to the threat-anticipation task was unrelated to variation in N/NE, regardless of threat certainty (uncertain, $\beta = -0.10$; $t_{(217)} = -0.99$; $p = 0.32$; certain, $\beta = 0.04$; $t_{(217)} = 0.45$; $p = 0.65$; Fig. 8e,f). EAc reactivity to the threat-perception (emotional-faces) task was also unrelated to N/NE (BST, $\beta = 0.03$; $t_{(211)} = 0.38$; $p = 0.70$; Ce, $\beta = 0.03$; $t_{(211)} = 0.37$; $p = 0.72$; Fig. 8g,h). Consistent with these nil effects, the association between BST reactivity to uncertain threat and N/NE remained significant in models that controlled for either Ce reactivity to uncertain-threat anticipation or BST reactivity to threat-related faces ($t > 2.59$; $p < 0.02$). The association between N/NE and BST reactivity to uncertain threat was significantly greater than that obtained for Ce reactivity to uncertain threat ($t_{\text{Hotelling}(217)} = 2.94$; $p = 0.004$), but did not differ from that obtained for BST reactivity to threat-related faces ($t_{\text{Hotelling}(206)} = 1.57$; $p = 0.12$). In sum, across the regions and tasks considered here, individual differences in N/NE are uniquely associated with heightened BST activation during the uncertain anticipation of a genuinely distressing threat (Fig. 9).
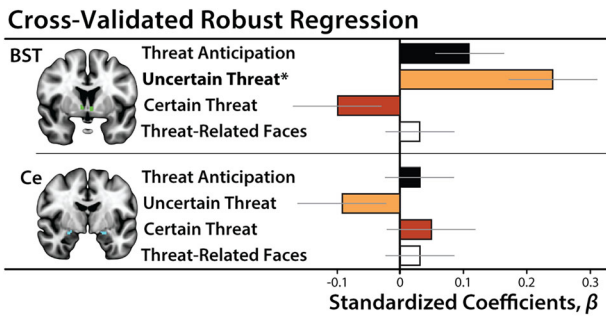
BST reactivity to uncertain threat is broadly associated with the "internalizing" facets of N/NE

Epidemiological, psychiatric, and biological studies typically focus on coarse "broadband" measures of N/NE (Shackman et al., 2016; Hur et al., 2019). Yet it is clear that N/NE is a complex phenotype that subsumes several narrower traits—including dispositional anxiety, depression/sadness, and emotional volatility (Caspi et al., 2005; Soto and John, 2017; Kalokerinos et al., 2020)_ENREF_16—each characterized by a mixture of shared and unique psychological associations and biological correlates (Thorp et al., 2021; Klein-Flügge et al., 2022; Watson et al., 2022; Khoo et al., 2023). While our composite N/NE instrument has many psychometric strengths (Fig. 1), it cannot address which of these facets is the most relevant to BST function (McCrae, 2015). To do so, we leveraged the revised BFI-2, a well-established, hierarchically organized scale that was expressly constructed to enable rigorous facet-level analyses (Soto and John, 2017). The BFI-2 was administered at the baseline (T2) and
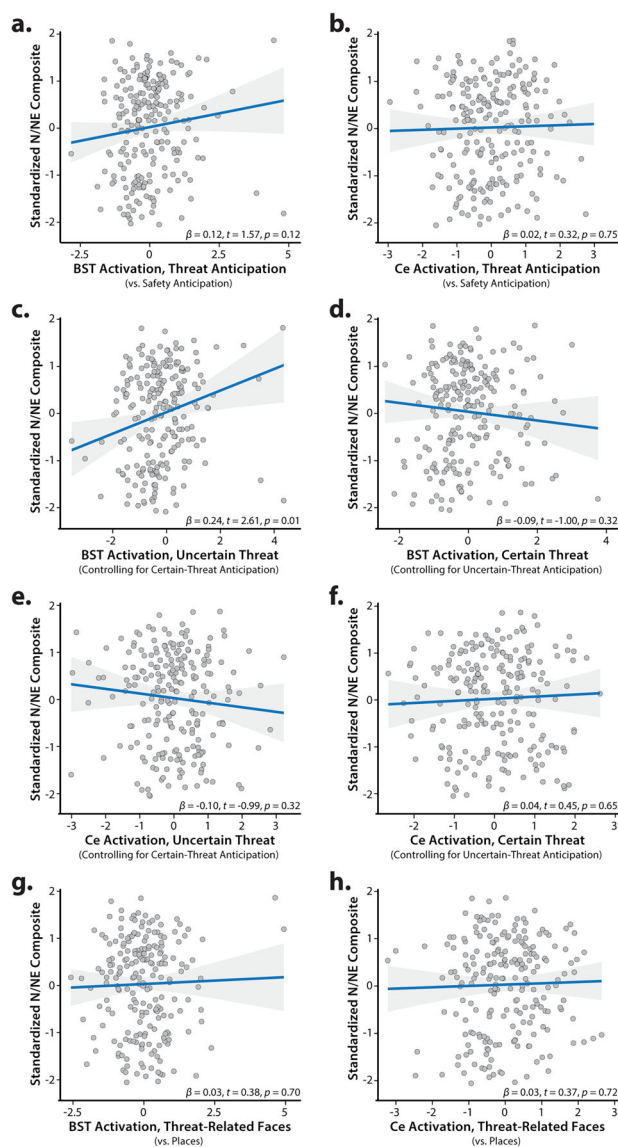
Figure 8. Individual differences in N/NE are associated with heightened BST activation during the uncertain anticipation of a genuinely distressing threat. Scatterplots depict the robust association (blue line) between N/NE (standardized multiscale/multioccasion composite) and each task-related neuroimaging metric for the BST and Ce ROIs. Panels c–f depict partial correlations. Panels a–b and g–h depict standard correlations. Activation estimates for the anticipation of certain/uncertain threat and the presentation of threat-related faces reflect differences relative to the implicit baseline. Gray bands indicate 95% confidence intervals. BST, bed nucleus of the stria terminalis ROI; Ce, central nucleus of the amygdala ROI; N/NE, neuroticism/negative emotionality.

6 month follow-up (T3) sessions (Fig. 1). Paralleling the approach used for broadband N/NE, facet scores were averaged across assessments to minimize occasion-specific fluctuations ("noise"). Cross-validated robust GLMs were used to quantify associations between BST reactivity to uncertain-threat anticipation and each facet of N/NE while controlling for BST reactivity to certain threat. Results revealed significant associations with dispositional anxiety and depression/sadness, but not emotional volatility (anxiety, $\beta = 0.20$; $t_{(217)} = 2.19$; $p = 0.03$; depression/sadness, $\beta = 0.22$; $t_{(217)} = 2.45$; $p = 0.02$; volatility, $\beta = 0.10$; $t_{(217)} = 1.10$; $p = 0.27$). Consistent with the broadband results, BST reactivity to certain-threat anticipation was unrelated to the three narrow traits ($p > 0.21$). In cross-validated bivariate models, variation in BST reactivity to uncertain-threat anticipation

Cross-Validated Robust Regression

Figure 9. Summary of robust-regression models. Heightened BST reactivity to uncertain-threat anticipation (orange) was associated with elevated levels of N/NE ($p = 0.01$). Other associations were not significant ($p > 0.11$). Bars depict standardized coefficients for each robust-regression model. Whiskers indicate standard errors. Significant associations are marked by an asterisk. BST, bed nucleus of the stria terminalis ROI; Ce, central nucleus of the amygdala ROI.

Table 2. Convergent validity of EAc reactivity to the threat-anticipation and threat-perception paradigms (anatomically defined ROIs; spatially unsmoothed data)

ROI	Contrast A[a]	Contrast B[a]	Robust β	$t_{(207)}$[b]	Nominal p
BST	Threat-related faces	Threat anticipation	0.11	1.80	0.07
		Uncertain-threat anticipation	0.02	0.42	0.68
		Certain-threat anticipation	0.12	1.68	0.10
Ce	Threat-related faces	Threat anticipation	−0.01	−0.20	0.84
		Uncertain-threat anticipation	−0.10	−1.47	0.14
		Certain-threat anticipation	−0.11	−1.54	0.12

BST, bed nucleus of the stria terminalis; Ce, dorsal amygdala in the region of the central nucleus; EAc, central extended amygdala; ROI, region of interest.
[a]Relative to their respective reference conditions.
[b]A total of 209 participants provided usable data for both paradigms.

explained an average of ∼4% of the variance in the anxiety and depression/sadness facets of N/NE in out-of-sample test data (anxiety, $\beta = 0.15$; $t_{(218)} = 2.13$; $p = 0.04$; cross-validated $R^2 = 0.041$; depression/sadness, $\beta = 0.16$; $t_{(218)} = 2.17$; $p = 0.03$; cross-validated $R^2 = 0.040$). While the BST is often conceptualized as playing a central role in anxiety-related states, traits, and disorders (Fox and Shackman, 2019; Shackman and Fox, 2021; Grogans et al., 2023), these findings demonstrate that heightened BST reactivity to uncertain threat is more broadly associated with the "internalizing" facets of N/NE (anxiety and depression/sadness). They also indicate that our major conclusions generalize across questionnaire instruments.

EAc reactivity to the threat-anticipation and threat-perception tasks shows negligible convergence

It is often assumed that different experimental manipulations of "threat" are fungible probes of individual differences in circuit function (i.e., threat-of-shock ≈ threat-related faces). Yet this tacit assumption of convergent validity has never been tested in a larger sample or in the BST (Villalta-Gil et al., 2017). As shown in Table 2, robust GLMs revealed negligible associations between BST reactivity to the threat-anticipation and threat-perception (emotional-faces) tasks ($p > 0.06$). The same pattern of null associations was evident for the Ce ($p > 0.11$). The absence of robust cross-task correlations raises important questions about the equivalence of two popular fMRI threat tasks—one centered on the cued anticipation of aversive stimulation and the other focused on the perception of angry and fearful facial expressions—and caution against relying exclusively on emotional-face paradigms to probe individual differences in threat-related EAc function (Grogans et al., 2022).

Discussion

Our results show that the Maryland Threat Countdown paradigm elicited robust distress and arousal, confirming its validity as a N/NE-relevant challenge (Fig. 5). Fearful and anxious feelings were more intense and indiscriminate among high-N/NE individuals, with elevated distress apparent even while waiting for benign stimulation (Fig. 6). Both threat paradigms strongly recruited the EAc, indicating that our approach is appropriate for probing its function (Figs. 5, 7). Cross-validated robust regressions showed that N/NE is associated with heightened BST activation during the temporally uncertain anticipation of threat (Figs. 8, 9). In contrast, N/NE was unrelated to BST activation during certain-threat anticipation, Ce activation during either type of threat anticipation, or BST/Ce reactivity to threat-related faces. While the BST is often conceptualized in terms of anxiety, our results suggest that it is broadly associated with the internalizing facets of N/NE, including the tendency to experience sadness and depression. While it is often assumed that different threat paradigms are interchangeable measures of individual differences in EAc function, our results revealed negligible cross-task associations in the EAc (Table 2).

Our results show that N/NE is associated with heightened BST reactivity to uncertain-threat anticipation, extending prior work (Shackman et al., 2016). Differences in N/NE are heritable, and work in monkeys suggests that variation in BST reactivity to uncertain threat is particularly relevant to the heritable component of N/NE (Fox et al., 2015a), although we acknowledge that it remains unknown whether this association is specific to uncertain-threat anticipation or reflects a broader hypersensitivity to uncertainty (Grupe and Nitschke, 2013). Anatomical tracing studies indicate that the BST is poised to assemble behavioral, psychophysiological, and neuroendocrine signs of negative affect via projections to downstream effectors (Fox et al., 2015b). Collectively, these observations reinforce the hypothesis that the BST is an evolutionarily conserved component of the distributed neural system governing trait-like individual differences in threat reactivity. A key challenge will be to clarify causation. Although the mechanistic contribution of the BST to dispositional fear and anxiety has yet to be explored in primates, work in rodents shows that the BST exerts bidirectional control over defensive behaviors triggered by uncertain-threat anticipation (Jennings et al., 2013; S. Y. Kim et al., 2013; Glangetas et al., 2017; Ahrens et al., 2018; Mazzone et al., 2018). Among humans, N/NE is stable but can change in response to experience, providing opportunities for understanding causation (Stieger et al., 2021; Zemestani et al., 2022). In a comprehensive meta-analysis, Roberts and colleagues documented substantial N/NE reductions following treatment for internalizing disorders (Roberts et al., 2017). It will be fruitful to determine whether this reflects dampened BST reactivity to uncertain threat and whether it depends on treatment modality (i.e., psychosocial vs pharmacological).

Elevated N/NE is a prominent risk factor for pathological anxiety and depression (Shackman et al., 2016; Toenders et al., 2022). Comorbidity between anxiety and depression disorders is rampant and ∼75% of patients with major depression exhibit significant anxiety symptoms (Hasin et al., 2018; Caspi et al., 2020). Furthermore, anxiety, depression, and N/NE show robust genetic

correlations and parallel pharmacological effects (Barlow et al., 2013; Levey et al., 2020; Thorp et al., 2021). Although these findings suggest a common neurobiological substrate (Barlow et al., 2013), identifying the relevant circuitry has proven challenging (Grogans et al., 2022). Our observation that heightened BST reactivity to uncertain threat is associated with both the anxious and the depressive facets of N/NE suggests that alterations in BST threat reactivity might contribute to this still-enigmatic shared substrate. While this hypothesis remains untested, the available evidence is supportive. A recent meta-analysis demonstrated that the BST is hyper-reactive to unpleasant emotional challenges among individuals with anxiety disorders (Chavanne and Robinson, 2021). Both anxiety and depression are often treated via chronic administration of selective serotonin reuptake inhibitors or, in the case of anxiety, acute administration of benzodiazepines. Both treatments have been shown to disproportionately reduce defensive responses to uncertain threat (relative to certain threat) in humans and rats and to dampen BST reactivity to uncertain threat in rats (Bechtholt et al., 2008; Grillon and Ernst, 2020). A key avenue for future research will be to use prospective-longitudinal data to test whether exaggerated BST activation during uncertain-threat anticipation increases the likelihood of future anxiety and depression.

Our results have implications for the design and interpretation of neuroimaging studies of psychiatric risk, disease, and treatment. Most of this work relies on emotional-face tasks as the lone probe of fear, anxiety, and related "Negative Valence Systems." Yet our results indicate that Ce and BST reactivity to threat-related faces is unrelated to the risk-conferring N/NE phenotype. These null effects are not unprecedented. Three other well-powered studies failed to detect associations between amygdala face reactivity and N/NE (MacDuffie et al., 2019; Silverman et al., 2019; West et al., 2021). Our results also make it clear that the acute perception of threat-related faces and the anticipation of aversive stimulation are statistically distinct assays of individual differences in EAc function, consistent with prior work in a much smaller sample (Villalta-Gil et al., 2017). These observations highlight the hazards of continuing to rely on a limited number of "workhorse" neuroimaging paradigms to understand and predict emotion, temperament, and psychopathology (Grogans et al., 2023). They also caution against muddling the distinction between the perception of threat-related cues and the actual experience of fear and anxiety, a practice that has become routine in experimental therapeutics research (Kwako et al., 2015; Schwandt et al., 2016; Paulus et al., 2021; Bloomfield et al., 2022).

Our results indicate that BST reactivity to uncertain threat predicts 5.1% of the variance in N/NE in out-of-sample data. The magnitude of this association—while too modest for practical applications—appears plausible, given the complexity of the N/NE phenotype and BST function, and compares favorably with other psychiatrically relevant associations, including prospective associations between striatal reward reactivity and depression (1%) and amygdala face reactivity and internalizing symptoms (2.7%; Grogans et al., 2022). It exceeds the predictive performance (1.5–4.2%) of polygenic scores derived from large-scale GWAS of N/NE (Nagel et al., 2018; Baselmans et al., 2019). Notably, the magnitude of our BST "hit" is half that of the cross-validated association reported for dorsal-attention network activation during a working-memory paradigm and general-cognitive ability (11.6%), suggesting that it is not unrealistically large (Marek et al., 2022). From a mechanistic perspective, the small-but-reliable hits uncovered by adequately

powered association studies are useful for prioritizing targets for perturbation studies. This reflects the fact that modest brain–behavior associations do not preclude substantially larger effects with targeted interventions (Shackman and Fox, 2018). Indeed, EAc damage can have dramatic consequences for fear- and anxiety-related states and traits (Fox and Shackman, 2019).

Our results also have implications for psychological theories of N/NE. Most theories are rooted in the idea that N/NE reflects hypersensitivity to threat, amplifying emotional responses when stressors are encountered (Spielberger, 1966; Eysenck, 1967; Kagan et al., 1988). Indeed, we found that high-N/NE individuals experienced potentiated distress when anticipating threat relative to safety ($R^2 = 2.9\%$; Fig. 6b). Yet high-N/NE individuals also reported heightened distress when anticipating outcomes—whether aversive or benign—that were simply uncertain ($R^2 = 2.6\%$; Fig. 6c), consistent with models emphasizing the centrality of uncertainty to anxiety (Grupe and Nitschke, 2013). But by far the strongest effect of N/NE was indiscriminately elevated distress across threat and safety trials ($R^2 = 13.7\%$; Fig. 6a). This finding is consistent with other work using threat-anticipation paradigms (Sep et al., 2019; Stegmann et al., 2019) and extends research focused on more naturalistic provocations (e.g., aversive films) and smartphone measures of real-world experience (Shackman et al., 2016; Hur et al., 2022). Collectively, these observations reinforce models that emphasize the importance of pervasive, contextually inappropriate negative affect (Shackman et al., 2016). From a psychiatric perspective, overgeneralized responses to threat are particularly noteworthy because they promote avoidance, a key feature of pathological anxiety; distinguish patients from controls; and confer risk for future psychopathology (Shackman et al., 2016; Hunt et al., 2017).

Clearly, important challenges remain. First, our study was focused on an ethnoracially diverse sample of emerging adults. Moving forward, it will be important to extend this to more representative samples. Second, although our results highlight the importance of the BST, N/NE is a complex, multidimensional phenotype that undoubtedly reflects multiple regions and networks. It will be important to understand how interactions between the BST and other regions implicated in the expression and regulation of negative affect support variation in N/NE. Third, the absence of reward trials precludes strong claims about valence. While unlikely, similar associations might be evident for uncertain-reward anticipation. Fourth, BST function was unrelated to task-related distress, raising questions about the precise mechanisms linking it to variation in N/NE. This null association might reflect an artifact of our sparse distress-sampling protocol (16.7% trials) or it could be that BST reactivity to uncertain-threat anticipation only indirectly influences conscious feelings (Taschereau-Dumouchel et al., 2022). Moving forward, it will be useful to collect trial-by-trial fear/anxiety ratings, enabling formal mediation analyses, and to assess relations with real-world distress.

Elevated N/NE is associated with a multitude of practically important outcomes, yet the underlying neurobiology has remained unclear. Our observations show that N/NE is associated with heightened activation during the anticipation of an uncertain, genuinely distressing threat in the BST, but not in the Ce. EAc reactivity to threat-related faces was also unrelated to N/NE. These observations provide a neurobiological framework for conceptualizing N/NE and set the stage for more ambitious prospective-longitudinal and mechanistic studies. A comparatively large, diverse, and carefully phenotyped sample and a preregistered, best-practices approach enhance confidence in these results.

Data Availability

Raw data and select materials are publicly available at the National Institute of Mental Health Data Archive (https://nda.nih.gov/edit_collection.html?id=2447). Processed data and supplementary tables (e.g., cluster tables) are available at the Open Science Framework (https://osf.io/w5cdk). Key neuroimaging maps are available at NeuroVault (https://neurovault.org/collections/13109).

References

Ahrens S, Wu MV, Furlan A, Hwang GR, Paik R, Li H, Penzo MA, Tollkuhn J, Li B (2018) A central extended amygdala circuit that modulates anxiety. J Neurosci 38:5567–5583.

Allen M, Poggiali D, Whitaker K, Marshall T, Kievit RA (2021) Raincloud plots: a multi-platform tool for robust data visualization. Wellcome Open Res 4:63.

Avants BB, Tustison NJ, Song G, Cook PA, Klein A, Gee JC (2011) A reproducible evaluation of ANTs similarity metric performance in brain image registration. Neuroimage 54:2033–2044.

Bach DR, Castegnetti G, Korn CW, Gerster S, Melinscak F, Moser T (2018) Psychophysiological modeling: current state and future directions. Psychophysiology 55:e13214.

Bach DR, Flandin G, Friston KJ, Dolan RJ (2010) Modelling event-related skin conductance responses. Int J Psychophysiol 75:349–356.

Bach DR, Friston KJ (2013) Model-based analysis of skin conductance responses: towards causal models in psychophysiology. Psychophysiology 50:15–22.

Baranger DAA, Lindenmuth M, Nance M, Guyer AE, Keenan K, Hipwell AE, Shaw DS, Forbes EE (2021) The longitudinal stability of fMRI activation during reward processing in adolescents and young adults. Neuroimage 232:117872.

Barlow DH, Sauer-Zavala S, Carl JR, Bullis JR, Ellard KK (2013) The nature, diagnosis, and treatment of neuroticism: back to the future. Clin Psychol Sci 2:344–365.

Bas-Hoogendam JM, et al. (2022) Structural brain correlates of childhood inhibited temperament: an ENIGMA-anxiety mega-analysis. J Am Acad Child Adolesc Psychiatry 61:1182–1188.

Baselmans BML, et al. (2019) Multivariate genome-wide analyses of the well-being spectrum. Nat Genet 51:445–451.

Bechtholt AJ, Valentino RJ, Lucki I (2008) Overlapping and distinct brain regions associated with the anxiolytic effects of chlordiazepoxide and chronic fluoxetine. Neuropsychopharmacology 33:2117–2130.

Bloomfield MAP, et al. (2022) The acute effects of cannabidiol on emotional processing and anxiety: a neurocognitive imaging study. Psychopharmacology 239:1539–1549.

Brinkmann L, Buff C, Feldker K, Neumeister P, Heitmann CY, Hofmann D, Bruchmann M, Herrmann MJ, Straube T (2018) Inter-individual differences in trait anxiety shape the functional connectivity between the bed nucleus of the stria terminalis and the amygdala during brief threat processing. Neuroimage 166:110–116.

Brown GG, et al. (2011) Multisite reliability of cognitive BOLD data. Neuroimage 54:2163–2175.

Caspi A, et al. (2020) Longitudinal assessment of mental health disorders and comorbidities across 4 decades among participants in the Dunedin birth cohort study. JAMA Netw Open 3:e203221.

Caspi A, Roberts BW, Shiner RL (2005) Personality development: stability and change. Annu Rev Psychol 56:453–484.

Charpentier CJ, et al. (2021) How representative are neuroimaging samples? Large-scale evidence for trait anxiety differences between fMRI and behaviour-only research participants. Soc Cogn Affect Neurosci 16:1057–1070.

Chavanne AV, Robinson OJ (2021) The overlapping neurobiology of adaptive and pathological anxiety: a meta-analysis of functional neural activation. Am J Psychiatry 178:156–164.

Conway CC, Grogans SE, Anderson AS, Islam S, Craig LE, Wedlock J, Hur J, DeYoung KA, Shackman AJ (in press) Neuroticism is selectively associated with longitudinal increases in broadband internalizing symptoms, but not narrow-band positive affect or anxious arousal, in emerging adulthood. Clin Psychol Sci.

Cox RW (1996) AFNI: software for analysis and visualization of functional magnetic resonance neuroimages. Comput Biomed Res 29:162–173.

Daldrup T, Remmes J, Lesting J, Gaburro S, Fendt M, Meuth P, Kloke V, Pape HC, Seidenbecher T (2015) Expression of freezing and fear-potentiated startle during sustained fear in mice. Genes Brain Behav 14:281–291.

Desikan RS, et al. (2006) An automated labeling system for subdividing the human cerebral cortex on MRI scans into gyral based regions of interest. Neuroimage 31:968–980.

DeYoung CG, et al. (2022) Personality neuroscience: an emerging field with bright prospects. Personal Sci 3:e7269.

Erdfelder E, Faul F, Buchner A (1996) GPOWER: a general power analysis program. Behav Res Methods Instrum Comput 28:1–11.

Eskildsen SF, Coupé P, Fonov V, Manjón JV, Leung KK, Guizard N, Wassef SN, Østergaard LR, Collins DL, Alzheimer's Disease Neuroimaging Initiative (2012) BEaST: brain extraction based on nonlocal segmentation technique. Neuroimage 59:2362–2373.

Eysenck HJ (1967) *The biological basis of personality*. Springfield, IL: Charles C. Thomas.

First MB, Williams JBW, Karg RS, Spitzer RL (2015) *Structured clinical interview for DSM-5—research version (SCID-5 for DSM-5, research version; SCID-5-RV)*. Arlington, VA: American Psychiatric Association.

Fox AS, et al. (2015a) Intergenerational neural mediators of early-life anxious temperament. Proc Natl Acad Sci U S A 112:9118–9122.

Fox AS, Lapate RC, Shackman AJ, Davidson RJ (2018) *The nature of emotion: fundamental questions*, Ed 2. New York, NY: Oxford University Press.

Fox AS, Oler JA, Tromp DP, Fudge JL, Kalin NH (2015b) Extending the amygdala in theories of threat processing. Trends Neurosci 38:319–329.

Fox AS, Shackman AJ (2019) The central extended amygdala in fear and anxiety: closing the gap between mechanistic and neuroimaging research. Neurosci Lett 693:58–67.

Frazier JA, et al. (2005) Structural brain magnetic resonance imaging of limbic and thalamic volumes in pediatric bipolar disorder. Am J Psychiatry 162:1256–1265.

Glangetas C, et al. (2017) NMDA-receptor-dependent plasticity in the bed nucleus of the stria terminalis triggers long-term anxiolysis. Nat Commun 8:14456.

Goldberg LR (1999) A broad-bandwidth, public domain, personality inventory measuring the lower-level facets of several five-factor models. In: *Personality psychology in Europe* (Mervielde I, Deary I, De Fruyt F, Ostendorf F, eds), pp 7–28. Tilburg, The Netherlands: Tilburg University Press.

Goldberg LR, Johnson JA, Eber HW, Hogan R, Ashton MC, Cloninger CR, Gough HC (2006) The international personality item pool and the future of public-domain personality measures. J Res Pers 40:84–96.

Grabner G, Janke AL, Budge MM, Smith D, Pruessner J, Collins DL (2006) Symmetric atlasing and model based segmentation: an application to the hippocampus in older adults. Med Image Comput Comput Assist Interv 9:58–66.

Grillon C, Ernst M (2020) A way forward for anxiolytic drug development: testing candidate anxiolytics with anxiety-potentiated startle in healthy humans. Neurosci Biobehav Rev 119:348–354.

Grogans SE, et al. (2023) The nature and neurobiology of fear and anxiety: state of the science and opportunities for accelerating discovery. Neurosci Biobehav Rev 151:105237.

Grogans SE, Fox AS, Shackman AJ (2022) The amygdala and depression: a sober reconsideration. Am J Psychiatry 179:454–457.

Grogans SE, Shackman AJ (2021) Understanding the relevance of extended amygdala reactivity to dispositional negativity [OSF pre-registration].

Grupe DW, Nitschke JB (2013) Uncertainty and anticipation in anxiety: an integrated neurobiological and psychological perspective. Nat Rev Neurosci 14:488–501.

Hasin DS, Sarvet AL, Meyers JL, Saha TD, Ruan WJ, Stohl M, Grant BF (2018) Epidemiology of adult DSM-5 major depressive disorder and its specifiers in the United States. JAMA Psychiatry 75:336–346.

Hauner KK, Zinbarg RE, Revelle W (2014) A latent variable model approach to estimating systematic bias in the oversampling method. Behav Res 46:786–797.

Hefner KR, Moberg CA, Hachiya LY, Curtin JJ (2013) Alcohol stress response dampening during imminent versus distal, uncertain threat. J Abnorm Psychol 122:756–769.

Heilicher M, Crombie KM, Cisler JM (2022) Test-retest reliability of fMRI during an emotion processing task: investigating the impact of analytical approaches on ICC values. Front Neuroimaging 1:859792.

Henson R (2007) Efficient experimental design for fMRI. In: *Statistical parametric mapping: the analysis of functional brain images* (Friston K,

Ashburner J, Kiebel S, Nichols T, Penny W, eds), pp 193–210. New York, NY: Academic Press.

Hotelling H (1940) The selection of variates for use in prediction with some comments on the general problem of nuisance parameters. Ann Math Stat 11:271–283.

Hunt C, Cooper SE, Hartnell MP, Lissek S (2017) Distraction/suppression and distress endurance diminish the extent to which generalized conditioned fear is associated with maladaptive behavioral avoidance. Behav Res Ther 96:90–105.

Hur J, et al. (2022) Anxiety-related frontocortical activity is associated with dampened stressor reactivity in the real world. Psychol Sci 33:906–924.

Hur J, DeYoung KA, Islam S, Anderson AS, Barstead MG, Shackman AJ (2020a) Social context and the real-world consequences of social anxiety. Psychol Med 50:1989–2000.

Hur J, Smith JF, DeYoung KA, Anderson AS, Kuang J, Kim HC, Tillman RM, Kuhn M, Fox AS, Shackman AJ (2020b) Anxiety and the neurobiology of temporally uncertain threat anticipation. J Neurosci 40:7949–7964.

Hur J, Stockbridge MD, Fox AS, Shackman AJ (2019) Dispositional negativity, cognition, and anxiety disorders: an integrative translational neuroscience framework. Prog Brain Res 247:375–436.

Indovina I, Robbins TW, Núñez-Elizalde AO, Dunn BD, Bishop SJ (2011) Fear-conditioning mechanisms associated with trait vulnerability to anxiety in humans. Neuron 69:563–571.

Infantolino ZP, Luking KR, Sauder CL, Curtin JJ, Hajcak G (2018) Robust is not necessarily reliable: from within-subjects fMRI contrasts to between-subjects comparisons. Neuroimage 173:146–152.

The jamovi project (2023) In. Sydney, Australia.

BIAC (2022) IXI dataset. London: Imperial College London.

Jenkinson M, Beckmann CF, Behrens TE, Woolrich MW, Smith SM (2012) FSL. Neuroimage 62:782–790.

Jennings JH, Sparta DR, Stamatakis AM, Ung RL, Pleil KE, Kash TL, Stuber GD (2013) Distinct extended amygdala circuits for divergent motivational states. Nature 496:224–228.

John OP, Naumann LP, Soto CJ (2008) Paradigm shift to the integrative big-five trait taxonomy: history, measurement, and conceptual issues. In: *Handbook of personality: theory and research* (John OP, Robins RW, Pervin LA, eds), pp 114–158, NY: Guilford.

Kafadar K (1983) The efficiency of the biweight as a robust estimator of location. J Res Natl Bur Stand 88:105–116.

Kagan J (2022) Temperamental and theoretical contributions to clinical psychology. Annu Rev Clin Psychol 18:1–18.

Kagan J, Reznick JS, Snidman N (1988) Biological bases of childhood shyness. Science 240:167–171.

Kalokerinos EK, et al. (2020) Neuroticism may not reflect emotional variability. Proc Natl Acad Sci U S A 117:9270–9276.

Kennedy JT, Harms MP, Korucuoglu O, Astafiev SV, Barch DM, Thompson WK, Bjork JM, Anokhin AP (2022) Reliability and stability challenges in ABCD task fMRI data. Neuroimage 252:119046.

Khoo S, Stasik-O'Brien SM, Ellickson-Larew S, Stanton K, Clark LA, Watson D (2023) The predictive validity of consensual and unique facets of neuroticism, conscientiousness, and agreeableness in five personality inventories. Assessment 30:1182–1199.

Kim SY, et al. (2013) Diverging neural pathways assemble a behavioural state from separable features in anxiety. Nature 496:219–223.

Kim HC, et al. (2023) Acute nicotine abstinence amplifies subjective withdrawal symptoms and threat-evoked fear and anxiety, but not extended amygdala reactivity. PLoS One 18:e0288544.

Kirlic N, Aupperle RL, Rhudy JL, Misaki M, Kuplicki R, Sutton A, Alvarez RP (2019) Latent variable analysis of negative affect and its contributions to neural responses during shock anticipation. Neuropsychopharmacology 44:695–702.

Klein-Flügge MC, Jensen DEA, Takagi Y, Priestley L, Verhagen L, Smith SM, Rushworth MFS (2022) Relationship between nuclei-specific amygdala connectivity and mental health dimensions in humans. Nat Hum Behav 1705–1722.

Klumpers F, Kroes MCW, Baas J, Fernandez G (2017) How human amygdala and bed nucleus of the stria terminalis may drive distinct defensive responses. J Neurosci 37:9645–9656.

Kruger O, Shiozawa T, Kreifelts B, Scheffler K, Ethofer T (2015) Three distinct fiber pathways of the bed nucleus of the stria terminalis to the amygdala and prefrontal cortex. Cortex 66:60–68.

Kuhn M, Wing J, Weston S, Williams A, Keefer C, Engelhardt A (2020) Caret: classification and regression training. R package version 6.0-86. 2020. Available at: http://CRAN R-project org/package=caret

Kwako LE, et al. (2015) The corticotropin releasing hormone-1 (CRH1) receptor antagonist pexacerfont in alcohol dependence: a randomized controlled experimental medicine study. Neuropsychopharmacology 40:1053–1063.

Lahey BB (2009) Public health significance of neuroticism. Am Psychol 64:241–256.

Lange MD, et al. (2017) Cannabinoid CB1 receptors in distinct circuits of the extended amygdala determine fear responsiveness to unpredictable threat. Mol Psychiatry 22:1422–1430.

Levey DF, et al. (2020) Reproducible genetic risk loci for anxiety: results from ~200,000 participants in the Million Veteran Program. Am J Psychiatry 177:223–232.

Lorio S, et al. (2016) New tissue priors for improved automated classification of subcortical brain structures on MRI. Neuroimage 130:157–166.

Love J, et al. (2019) JASP: graphical statistical software for common statistical designs. J Stat Softw 88:1–17.

MacDuffie KE, Knodt AR, Radtke SR, Strauman TJ, Hariri AR (2019) Self-rated amygdala activity: an auto-biological index of affective distress. Personal Neurosci 2:e1.

Makris N, Goldstein JM, Kennedy D, Hodge SM, Caviness VS, Faraone SV, Tsuang MT, Seidman LJ (2006) Decreased volume of left and total anterior insular lobule in schizophrenia. Schizophr Res 83:155–171.

Marek S, et al. (2022) Reproducible brain-wide association studies require thousands of individuals. Nature 603:654–660.

Maus B, van Breukelen GJ, Goebel R, Berger MP (2010) Optimization of blocked designs in fMRI studies. Psychometrika 75:373–390.

Mazzone CM, et al. (2018) Acute engagement of Gq-mediated signaling in the bed nucleus of the stria terminalis induces anxiety-like behavior. Mol Psychiatry 23:143–153.

McCormick M, Liu X, Jomier J, Marion C, Ibanez L (2014) ITK: enabling reproducible research and open science. Front Neuroinform 8:13.

McCrae RR (2015) A more nuanced view of reliability: specificity in the trait hierarchy. Pers Soc Psychol Rev 19:97–112.

Miles L, Davis M, Walker D (2011) Phasic and sustained fear are pharmacologically dissociable in rats. Neuropsychopharmacology 36:1563–1574.

Moberg CA, Bradford DE, Kaye JT, Curtin JJ (2017) Increased startle potentiation to unpredictable stressors in alcohol dependence: possible stress neuroadaptation in humans. J Abnorm Psychol 126:441–453.

Nagel M, et al. (2018) Meta-analysis of genome-wide association studies for neuroticism in 449,484 individuals identifies novel genetic loci and pathways. Nat Genet 50:920–927.

Nikolaidis A, Chen AA, He X, Shinohara RT, Vogelstein J, Milham M, Shou H (2022) Suboptimal phenotypic reliability impedes reproducible human neuroscience. bioRxiv.

Paulus MP, Stein MB, Simmons AN, Risbrough VB, Halter R, Chaplan SR (2021) The effects of FAAH inhibition on the neural basis of anxiety-related processing in healthy male subjects: a randomized clinical trial. Neuropsychopharmacology 46:1011–1019.

Plichta MM, et al. (2014) Amygdala habituation: a reliable fMRI phenotype. Neuroimage 103:383–390.

Poldrack RA, Baker CI, Durnez J, Gorgolewski KJ, Matthews PM, Munafò MR, Nichols TE, Poline J-B, Vul E, Yarkoni T (2017) Scanning the horizon: towards transparent and reproducible neuroimaging research. Nat Rev Neurosci 18:115–126.

Poldrack RA, Huckins G, Varoquaux G (2020) Establishment of best practices for evidence for prediction: a review. JAMA Psychiatry 77:534–540.

Poline J-B, Kherif F, Pallier C, Penny W (2007) Contrasts and classical inference. In: *Statistical parametric mapping: the analysis of functional brain images* (Friston KJ, Ashburner JT, Kiebel SJ, Nichols TE, Penny WD, eds), pp 126–139. London: Elsevier.

Pruim RHR, Mennes M, van Rooij D, Llera A, Buitelaar JK, Beckmann CF (2015) ICA-AROMA: a robust ICA-based strategy for removing motion artifacts from fMRI data. Neuroimage 112:267–277.

R Core Team (2022) R: a language and environment for statistical computing. Vienna, Austria: R Foundation for Statistical Computing.

Revelle W (2022) psych: Procedures for personality and psychological research. In: The Comprehensive R Archive Network (CRAN).

Roberts BW, Luo J, Briley DA, Chow PI, Su R, Hill PL (2017) A systematic review of personality trait change through intervention. Psychol Bull 143:117–141.

Roemer L, Lechner CM, Rammstedt B, Roberts BW (in press) The base-rate and longer-term relevance of year-to-year change in personality traits. Eur J Pers.

Rorden C (2019) MRIcron. In: NITRC.

RStudio Team (2022) RStudio: integrated development for R. Boston, MA: RStudio PBC.

Schuyler BS, et al. (2012) Temporal dynamics of emotional responding: amygdala recovery predicts emotional traits. Soc Cogn Affect Neurosci 9:176–181.

Schwandt ML, Cortes CR, Kwako LE, George DT, Momenan R, Sinha R, Grigoriadis DE, Pich EM, Leggio L, Heilig M (2016) The CRF1 antagonist verucerfont in anxious alcohol-dependent women: translation of neuroendocrine, but not of anti-craving effects. Neuropsychopharmacology 41:2818–2829.

Sep MSC, Steenmeijer A, Kennis M (2019) The relation between anxious personality traits and fear generalization in healthy subjects: a systematic review and meta-analysis. Neurosci Biobehav Rev 107:320–328.

Shackman AJ, Fox AS (2016) Contributions of the central extended amygdala to fear and anxiety. J Neurosci 36:8050–8063.

Shackman AJ, Fox AS (2018) Getting serious about variation: lessons for clinical neuroscience. Trends Cogn Sci 22:368–369.

Shackman AJ, Fox AS (2021) Two decades of anxiety neuroimaging research: new insights and a look to the future. Am J Psychiatry 178:106–109.

Shackman AJ, Fox AS, Oler JA, Shelton SE, Oakes TR, Davidson RJ, Kalin NH (2017) Heightened extended amygdala metabolism following threat characterizes the early phenotypic risk to develop anxiety-related psychopathology. Mol Psychiatry 22:724–732.

Shackman AJ, Grogans SE, Fox AS (in press) Fear, anxiety, and the functional architecture of the human central extended amygdala. Nat Rev Neurosci.

Shackman AJ, Tromp DPM, Stockbridge MD, Kaplan CM, Tillman RM, Fox AS (2016) Dispositional negativity: an integrative psychological and neurobiological perspective. Psychol Bull 142:1275–1314.

Shackman AJ, Weinstein JS, Hudja SN, Bloomer CD, Barstead MG, Fox AS, Lemay EP Jr (2018) Dispositional negativity in the wild: social environment governs momentary emotional experience. Emotion 18:707–724.

Silverman MH, Wilson S, Ramsay IS, Hunt RH, Thomas KM, Krueger RF, Iacono WG (2019) Trait neuroticism and emotion neurocircuitry: functional magnetic resonance imaging evidence for a failure in emotion regulation. Dev Psychopathol 31:1085–1099.

Sjouwerman R, Scharfenort R, Lonsdorf TB (2020) Individual differences in fear acquisition: multivariate analyses of different emotional negativity scales, physiological responding, subjective measures, and neural activation. Sci Rep 10:15283.

Somerville LH, Whalen PJ, Kelley WM (2010) Human bed nucleus of the stria terminalis indexes hypervigilant threat monitoring. Biol Psychiatry 68:416–424.

Soto CJ, John OP (2017) The next big five inventory (BFI-2): developing and assessing a hierarchical model with 15 facets to enhance bandwidth, fidelity, and predictive power. J Pers Soc Psychol 113:117–143.

Spielberger CD (1966) Theory and research on anxiety. In: *Anxiety and behavior* (Spielberger CD, ed), pp 3–22. NY: Academic Press.

Spisak T, Bingel U, Wager TD (2023) Multivariate BWAS can be replicable with moderate sample sizes. Nature 615:E4–E7.

Wellcome Centre for Human Neuroimaging (2022) SPM. London: University College London.

Stegmann Y, Reicherts P, Andreatta M, Pauli P, Wieser MJ (2019) The effect of trait anxiety on attentional mechanisms in combined context and cue conditioning and extinction learning. Sci Rep 9:8855.

Stieger M, Flückiger C, Rüegger D, Kowatsch T, Roberts BW, Allemand M (2021) Changing personality traits with the help of a digital personality change intervention. Proc Natl Acad Sci U S A 118:e2017548118.

Taschereau-Dumouchel V, Michel M, Lau H, Hofmann SG, LeDoux JE (2022) Putting the "mental" back in "mental disorders": a perspective from research on fear and anxiety. Mol Psychiatry 27:1322–1330.

Theiss JD, Ridgewell C, McHugo M, Heckers S, Blackford JU (2017) Manual segmentation of the human bed nucleus of the stria terminalis using 3 T MRI. Neuroimage 146:288–292.

Thorp JG, et al. (2021) Symptom-level modelling unravels the shared genetic architecture of anxiety and depression. Nat Hum Behav 5:1432–1442.

Tillman RM, Stockbridge MD, Nacewicz BM, Torrisi S, Fox AS, Smith JF, Shackman AJ (2018) Intrinsic functional connectivity of the central extended amygdala. Hum Brain Mapp 39:1291–1312.

Toenders YJ, et al. (2022) Predicting depression onset in young people based on clinical, cognitive, environmental, and neurobiological data. Biol Psychiatry Cogn Neurosci Neuroimaging 7:376–384.

Tozzi L, et al. (2020) The human connectome project for disordered emotional states: protocol and rationale for a research domain criteria study of brain connectivity in young adult anxiety and depression. Neuroimage 214:116715.

Tukey JW (1977) *Exploratory data analysis*. Reading, MA: Addison Wesley.

Tustison NJ, Avants BB, Cook PA, Zheng YJ, Egan A, Yushkevich PA, Gee JC (2010) N4ITK: improved N3 bias correction. IEEE Trans Med Imaging 29:1310–1320.

Villalta-Gil V, Hinton KE, Landman BA, Yvernault BC, Perkins SF, Katsantonis AS, Sellani CL, Lahey BB, Zald DH (2017) Convergent individual differences in visual cortices, but not the amygdala across standard amygdalar fMRI probe tasks. Neuroimage 146:312–319.

Visser RM, Bathelt J, Scholte HS, Kindt M (2021) Robust BOLD responses to faces but not to conditioned threat: challenging the amygdala's reputation in human fear and extinction learning. J Neurosci 41:10278–10292.

Wager TD, Keller MC, Lacey SC, Jonides J (2005) Increased sensitivity in neuroimaging analyses using robust regression. Neuroimage 26:99–113.

Watson D, Clark LA, Simms LJ, Kotov R (2022) Classification and assessment of fear and anxiety in personality and psychopathology. Neurosci Biobehav Rev 142:104878.

West HV, Burgess GC, Dust J, Kandala S, Barch DM (2021) Amygdala activation in cognitive task fMRI varies with individual differences in cognitive traits. Cogn Affect Behav Neurosci 21:254–264.

Wickham H (2016) *Ggplot2: elegant graphics for data analysis*, Ed 2. New York, NY: Springer-Verlag.

Wrzus C, Luong G, Wagner GG, Riediger M (2021) Longitudinal coupling of momentary stress reactivity and trait neuroticism: specificity of states, traits, and age period. J Pers Soc Psychol 121:691–706.

Yarkoni T, Westfall JA (2017) Choosing prediction over explanation in psychology: lessons from machine learning. Perspect Psychol Sci 12:1100–1122.

Yu C, Yao W (2017) Robust linear regression: a review and comparison. Commun Stat Simul Comput 46:6261–6282.

Zemestani M, Ommati P, Rezaei F, Gallagher MW (2022) Changes in neuroticism-related constructs over the unified protocol for transdiagnostic treatment of emotional disorders in patients on an optimal dose of SSRI. Personal Disord 13:171–181.

Zhu Y, et al. (2024) Distinct circuits from the central lateral amygdala to the ventral part of the bed nucleus of stria terminalis regulate different fear memory. Biol Psychiatry 95:732–744.